An improved model for the time-dependent material response of wood under mechanical loading and varying humidity conditions

Taoyi Yu [a,*], Ani Khaloian [a], Jan-Willem van de Kuilen [a,b]

[a] *Wood Technology, TUM School of Engineering and Design, Department of Materials Engineering, Technical University of Munich, Munich, Germany*
[b] *Biobased Structures and Materials, Faculty of Civil Engineering and Geosciences, Delft University of Technology, Delft, Netherlands*

ARTICLE INFO

ABSTRACT

Timber is one of the most widely applied engineering materials due to its favorable physical and mechanical characteristics. Nevertheless, over the service life, the combination of mechanical load and varying environmental conditions can have a critical influence on the mechanical response of timber structures, considering especially the mechano-sorptive characteristics. In this work, the performance analysis of the existing time- and moisture-dependent models identifies the need of a more comprehensive 3D constitutive rheological model, which can take into account orthotropic, elastic-plastic, viscoelastic and mechano-sorptive aspects, including the complex mechano-sorptive recovery phases that may occur over the lifetime. Therefore, a comprehensive algorithm of such a model is developed here. An improvement is made for the mechano-sorptive component by introducing an ordinary and a transcending mechano-sorptive part, which are governed by the absolute change of moisture content and the change exceeding the historical highest moisture content at each loading phase, respectively. Simulations are run under cases with mechanical loading of tension and compression perpendicular and parallel to the direction of the fibers. Both medium-term (up to 2500 h) as well as short-term (up to 350 h) mechanical behavior of the material under constant temperature is analyzed and good agreements are achieved with literature results. Comparison with existing models indicates that the proposed model gives an improved prediction of the mechano-sorptive creep and recovery, which has a non-linear dependence on the moisture history. Furthermore, sensitivity analyses are performed and the applicability of the model to different species under different combinations of load and moisture variation is studied here.

1. Introduction

Wood is an anisotropic, elasto-plastic, viscoelastic, hygroscopic material. During the service life of a timber structure, the material is subjected to an interaction of mechanical loads and environmental influences such as humidity variations. Since 1960s, experimental works [1] proved a strong influence of moisture variation on viscoelasticity, which is known as mechano-sorption or mechano-sorptive creep (MS). It is observed that the MS of wood is in general greater than the pure viscoelastic creep [2]. As a consequence, the combination of mechanical loading, moisture variation, and the time-to-failure effect can cause initiation of damage in timber elements and may lead to structural failure. An example of such structural failure was the collapse of the ice-hall Bad Reichenhall [3]. Other examples of structural failures can be found in the study of Frühwald et al. [4]. Moreover, besides the possible

catastrophic problems, the loading combinations are of general interest for structural assessment, where the load carrying capacity has to be analyzed [5]. Current modification factors like those given in EC5 [6] are strong simplifications regarding time-dependence loading as well as the humidity influence on both elasto-plastic and the long-term creep deformations. Hence, an in-depth research of the mechanical response of the materials and development of a material model that predicts their mechanical behavior can provide a guide for selecting more appropriate modification factors and play an important role in safety assessments of timber structures.

In order to study wood mechanical behavior, the microstructure of wood needs to be understood. Wood cell wall consists of different layers, among which the secondary wall is the thickest and is believed to have major influence on physical and mechanical properties. This layer is further divided into three layers, called S1, S2, and S3 layers. Each layer

---

has micro-fibrils aligned in a different angle. The thickest S2 layer dominates the cell behavior [7]. Most mechanical properties of wood can be explained by the chemical and physical interactions at wood cell level. However, the underlying mechanisms of MS remain somewhat unclear. Multiple theories, including hydrogen-bonding [8], deformation kinetics [9], lenticular trellis model [10], and slip-plane [11], were proposed to explain the micro-mechanism of the time- and moisture-dependent behavior of wood. Subsequently, analytical models based on these theories were developed [9,12–15]. These models offer good quantitative illustrations of the theories, yet, due to the complexity of mathematical equations and the great number of parameters, most of them turned out to be very laborious and facing difficulty for practical application or 3D generalization.

On the other hand, phenomenological models of the time- and moisture-dependent wood behavior have been extensively studied. The first development of a phenomenological model dealing with MS behavior dated back to the 70s [16,17], in which MS creep is modeled analogously as pure viscoelastic creep but driven by moisture accumulation. Different following-up model constructions, including Kelvin-type, co-excitation, Maxwell-type, and hydro-locking models, are developed according to the observed wood behavior under specific loading and environmental conditions, hence capable of capturing viscoelastic and MS characteristics to different extents [13,18]. An in-depth performance analysis of different models is given in this study, the differences and gaps between models are identified, and the possible limitations are discussed. The complexity of modelling MS creep, in comparison to the pure viscoelastic creep, lies in its non-linearity with moisture change and dependence on the moisture accumulation history. Besides the different MS creep rates at desorption and adsorption phases, a strong non-linearity is observed when wood is humidified to a moisture content exceeding the threshold experienced at the current load level (both at loading and unloading phases). The phenomenon is first documented in the study of Armstrong and Christensen [1] and widely observed in experiments [17,19–21]. Based on the work of Toratti [22], this work proposed a modified model addressing this phenomenon. Finally, a generalized 3D orthotropic elastic-plastic viscoelastic mechano-sorptive model for wood is developed, which covers the timber behavior under varying moisture conditions during loading and unloading phases. The proposed model is implemented in the finite element code ABAQUS/Standard via a user subroutine UMAT.

2. Review of rheological models

2.1. Introduction

Attempts for constructing rheological models including mechano-sorptive behavior dated back to the 1970s [16,17]. After validation of those models for specific species, the models have been implemented to assess the mechanical response of the material for a wide range of engineering applications [23–26]. A review of wood rheological models, primarily on one-dimension, was provided in the work of Hanhijärvi [18]. In this work, an overview including the further developments in the new century is given, including generalization to three-dimension [27–29], modification of constitutive laws [30,31], introduction of new elements/mechanisms [32,33], etc.

A summary of the evolution of modelling methods in the last decades is shown in Table 1, where the models are classified into serial type, parallel type, structure-based type, and hydro-lock type. These categories are not mutually exclusive. The Serial and parallel type refer to the models where elements (spring, dashpot, etc.) are assembled in serial or parallel, respectively. The structure-based type includes the models that developed according to the explanatory micro-mechanisms.

2.2. Single dashpot

Since mechano-sorption exhibits similar features to the time-

dependent normal creep, a "spring and dashpot" model was first proposed [16], shown in Table 1, in which the accumulated absolute moisture change $|\Delta u|$ is used as a substitute for the increment of time, as shown in equation (2.1):

$$\Delta \varepsilon^{ms} = a\sigma |\Delta u| \tag{2.1}$$

where ε^{ms}, a, and σ represent mechano-sorptive strain, compliance of mechano-sorptive creep, and stress, respectively. The compliance a can be given different values, for example, three values ($a+$, $a-$, and $a++$) to address the different MS creep rate during adsorption, desorption, and for the first change $\Delta u > 0$ in equation (2.2), respectively [17]. On the other hand, by using different compliance values for compression and tension situations, it can take into account the fact that MS is more pronounced under compression [34] as well.

$$a = \begin{cases} a^+, & if \, \Delta u > 0 \\ a^-, & if \, \Delta u < 0 \\ a^{++}, & for \, the \, first \, change \, \Delta u > 0 \end{cases} \tag{2.2}$$

However, a simple linear dashpot is not able to capture the recovery after unloading [17] or the MS creep limit [35]. Efforts of introducing recovery can be found in the studies of Mårtensson [36] and Ranta-Maunus [17]. As an example, an extra recovery compliance L is used in addition to MS creep compliance in the integral function in the work of Ranta-Maunus [17]. On the other hand, a strain-dependent mechano-sorptive parameter is utilized in the study of Mårtensson [20] to address the MS creep limit. Nevertheless, Santaoja [27] developed a three-dimensional constitutive model based on the simple linear dashpot, admitting the incapability in capturing the recovery. On this basis, Qiu [33] developed a rheological model taking also the damage mechanism [37] into consideration. In the works of Zhou et al.[23] and Qiu [33], applications of the 3D model for stress assessment in curved glulam can be found.
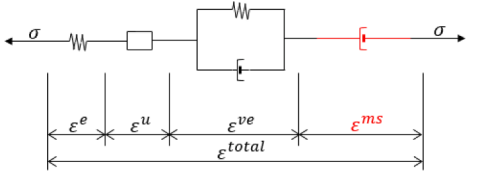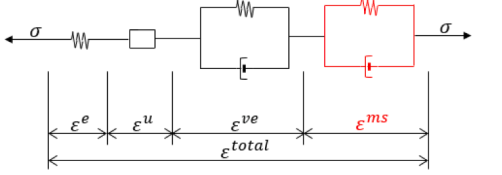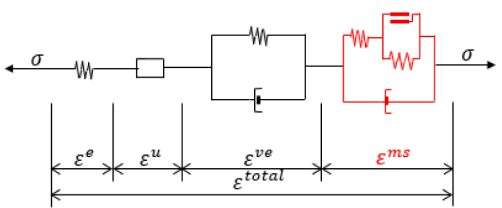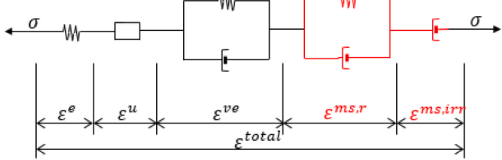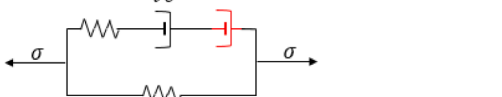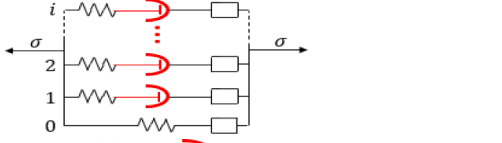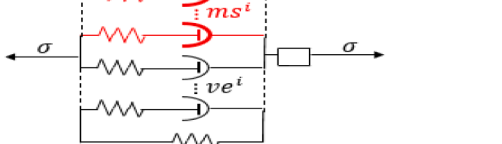
2.3. (Generalized) Kelvin-Voigt model

According to Hunt [38], the gradual exhaustion of the possible internal mechanisms of MS creep during moisture cycling can give an exponential approach to a MS creep limit, which resembles an analogous Kelvin-Voigt element (Table 1). Later on, the differential form of Kelvin-Voigt MS element was developed by Salin and Yahiaoui [39,40] and the integral form by Toratti [22]. A single MS Kelvin-Voigt component was used in the model of Becker [41], where the stiffness of the MS spring is modified to be moisture-history dependent. Extension of MS Kelvin-Voigt model into 2D (radial and tangential direction) can be found in the work of Mårtensson [42]. This model showed satisfactory estimation of drying stress on the cross-section and was later combined with moisture transport model for application to the full sized timber [43]. Huč [44] developed a 2D viscoelastic mechano-sorptive model taking into account the time-dependent Poisson's ratio. Based on the 3D formulation work of Fortino et al. [28], Hassani et al. [32] developed a rheological model associated with multi-surface plasticity model, where four Kelvin-Voigt elements for viscoelasticity and three Kelvin-Voigt elements for mechano-sorption are adopted and all material constants are defined as a function of moisture content.

2.4. Modified Kelvin-type model

One of the inherent properties of the above Kelvin-Voigt element is that all the generated strain is fully recoverable, which, is however not the case for wood [45]. Hence, to better predict the partially recoverable MS strains, modifications of the Kelvin-type models were reported in several researches [22,45]. One approach of modification [45] is based on the assumption that the irrecoverable MS creep (ε^{ir}) is in proportion to the total MS creep (ε^{ms}). The evolution of ε^{ir} is defined in a four-

Table 1
Summary of time- and moisture-dependent wood models.

	Models	Main Feature	First proposal	Further development
Serial connected model	Single Dashpot	Capability: MS creep under loading condition Limitation: 1. No MS creep limit 2. No MS recovery	[16] In 1971	Introducing recovery term and varying compliance a-,a+,a++ [17] Considering difference under compression and tension [34] Introducing creep limit term [20] 3D generalization [23,27,36] 3D generalization combined with damage mechanism [33]
	Generalized Kelvin-Voigt	Capability: 1. MS creep under loading 2. MS creep limit Limitation: Only fully MS recovery	[38] in 1989	Rate form of constitutive equation [39,40] Integral form of constitutive equation [22] Moisture history related MS stiffness [41] 2D generalization [42] in 1997/ 3D generalization [77] 2D generalization with time-dependent Poisson's ratio [44] 3D generalization combined with plasticity [32]
	Modified Kelvin-type	Capability: 1. MS creep under loading 2. MS creep limit 3. Including the irrecoverable part MS recovery	[45] in 2000	2D generalization with MS-plastic element [30,66]
			[16] in 1971	Integral form, compression driven dashpot [22] Introducing U and u [19] 3D generalization of [19]'s model [28] Applications of [28]'s model [24–26]
Parallel connected model	Co-exitation	Main Feature: MS is seen as amplification of viscoelasticity	–	–
	Generalized Maxwell	Main Feature: Deformation kinetic theory Limitation: 1. Insufficient MS recovery 2. Large number of parameters	[47] in 1985	First explanation of MS through kinetic theory [9,78] A calibrated and applied model with 10 parallel chains using non-linear dashpots [12]
Micro-structured model		Main Feature: Parallel viscoelastic and MS dashpots Limitation: Insufficient recovery		P + Q parallel elements for viscoelastic and MS, associated with failure criterion [48] 3D generalization of [48]'s model [29,49]
	Micro-stress redistribution	Main Feature: Based on S1/S2 layer interaction theory Limitation: Sophisticated construction	[14,50] in 1986 and 1987	–

Table 1 (*continued*)

Models	Main Feature	First proposal	Further development
Hydro-lock			Incremental form with Hooke's and Bazant's law [55] Introducing hydro-lock spring and MS stress [31] Double heredity integral [56] Boxes model [54] Multiple model possibilities to incorporate hydro-lock effect [57] 3D formalization of [57]'s model [58]
Other	Capability: Describe +, -, and ++ effects Limitation: Auxiliary stress needed for MS recovery	[53] in 1988	
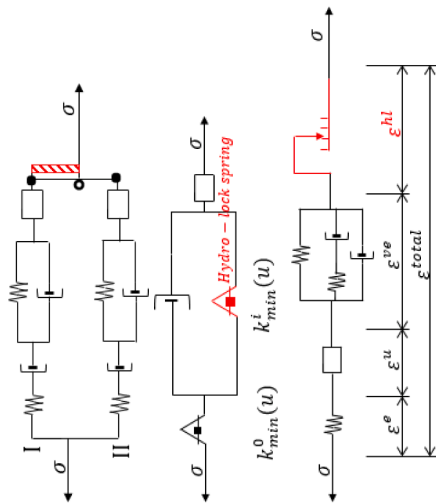
branched equation, based on conditions of moisture content, mechanical stress level, and strain history. Later on, a more concise model was developed using a so-called mechanosorptive-plastic element (Table 1), where the evolution of plastic deformation is controlled by orthotropic yield conditions [30]. With the return-mapping algorithm, the model was successfully implemented in 2D and was applied to simulate fast drying process.

The first idea of the second approach came up as early as 1971. Leicester [16] proposed graphically a two-unit MS model, where a dashpot and a series of Kelvin elements represent the irrecoverable and recoverable part of MS, respectively. Such a model (Table 1) was formalized in the work of Toratti [22], based on the assumption that the irrecoverable dashpot is only driven by compression load. In the study of Svensson and Toratti [19] the model was further calibrated for both long- and short-term tangential experiments. Different compared to what has been presented in the work of Toratti [22], the three Kelvin-Voigt elements are driven by the general moisture increment, denoted as du, yet the dashpot is only driven by the moisture increment that exceeds the previous threshold, denoted as dU. Based on this work, Fortino et al. [28] developed a 3D orthotropic viscoelastic mechanosorptive model combined with Fickian moisture transfer model. This model covers a wide range of MS characteristics using only linear Kelvin-Voigt and dashpot elements for MS part. Hence, it is further adopted for a series of wide applications[24–26] .

2.5. Co-excitation model

Experiments in the work of Hanhijärvi [18] indicated the existence of interaction between viscoelastic and MS creep mechanisms, possibly explainable by the physical ageing theory [46]. Consequently, a sketch of a co-excitation model (Table 1), instead of considering the two mechanisms separately as in Kelvin-type models, was proposed in their study. However, the practical effect of such co-excitation mechanism is not very strong [18].

2.6. Generalized Maxwell model

Similar to the Kelvin-type models, generalized Maxwell model is one of the most classical methods for describing the pure viscoelastic behavior as well. The earliest application of such model to wood MS creep can be found in the work of Bažant [47], where $f_v(|\dot{H}|)$, a function of moisture and temperature changing rate, is used to modify the viscosity of each dashpot element and a "ratchet" element is used to complete the recovery behavior. This model is purely theoretical and experimental validation is yet required to confirm the validity of the assumptions of Bažant [47].

The first explanation of MS effect using the deformation kinetics theory was given by Van der Put [9]. There, the moisture change is assumed to lower the activation energy for the hydrogen-bond reactions. In addition, mathematical derivation of a generalized Maxwell model is provided in his study. Later on, Hanhijärvi [12] adopted the idea and developed a model with 10 parallel chains (Table 1), containing elastic springs, non-linear dashpots, and hydro-expansion elements. MS is considered as a coupled effect of the non-linearity of the viscoelasticity and hydro-expansion process. With a couple of assumptions, such as a uniform spring stiffness value for nine parallel chains, it is claimed that the material parameters that are required for the model can be strongly reduced.

On the other hand, Bou Saïd [48] developed a non-linear generalized Maxwell model which is composed of parallel P + Q elements (Table 1), representing viscoelastic and MS creeps, respectively. The non-linearity is addressed by modifying the viscosity (η) as a function of stress level, moisture changing rate ($\dot{w}$), and moisture accumulation history (w_{hist}). This model is associated with failure criterion and softening mechanism. Such P + Q type of Maxwell model is further generalized into a 3D

model [29,49]. The validation tests showed good capability of capturing the non-linearity of creep at different structural scales, despite some insufficiencies in recovery and hydro-expansion oscillation estimation.

2.7. Micro-stress redistribution model

An interpretation of MS creep was proposed in the previous studies [14,50] that considers MS creep as being a result of redistribution of applied stress in the cell wall, due to the change of friction between the S1 and S2 layers induced by moisture content change. A corresponding model consisting of two parallel strings, whose stress redistribution is controlled by a hygroscopic bar, is developed (Table 1). As pointed out by Van der Put [9], this model is comparable to a two-parallel-Maxwell-element model containing non-linear dashpots based on another microscopic theory, deformation kinetics. Verifications of the model [14,50] can be found in the work of Mukudai and Yata [51], yet, the sophisticated process of load transfer between inner and outer cell-wall layers resulted in complex equations, which are difficult to be applied practically [52].

2.8. Hydro-lock model

Hydro-lock theory was first proposed in the studies of Gril [53] in order to reproduce the (+), (-), and (++) effects [17]. It assumes a temporary strain blocking in a drying phase under stress, which is possibly recoverable during humidifying. As summarized by Colmars et al. [54], the theory can be implemented by using the integral method or the discrete method. For the former method, Dubois et al. [55] proposed a generalized Kelvin-Voigt model using Hooke's law in humidifying and Bazant's law for describing the hardening behavior during drying phase. Later on, Husson et al. [31] developed the hydro-lock spring (Table 1) that retains the minimum stiffness corresponding to the mechanical and moisture load. Moreover, by introducing an auxiliary mechano-sorptive stress, they could solve the synchronizing difficulty that existed in the work of Dubois et al.[55]. Finally, a double heredity integral based on generalized Kelvin-Voigt model with hydro-lock spring was developed by Dubois et al. [56]. The latter discrete method, also called as box method, was initially proposed by Gril [53] using a mixed series/parallel box model. The model was modified and formalized by Colmars et al. [54] and was proved to be equivalent to the integral method. The existence of hydro-lock strain by mechano-sorptive experiments in the longitudinal direction is confirmed in the studies of Saifouni [57]. The first 3D hydro-lock model has been developed in Nguyen and Destrebecq [58], adopting the final model of Saifouni [57] to the longitudinal direction and assuming no hydro-lock effect on the other two directions.

2.9. Summary of the model overview

Mechano-sorption is a complex mechanism that is specially observed in wood. Several explanatory theories were proposed, some with microscopic evidence (hydrogen-bonding theory in Navi and Stanzl-Tschegg [59]), and some with verification models (deformation kinetics discussed in the study of Van der Put [9] and micro-stress redistribution in Mukudai and Yata [50]). However, none of the theories is thorough enough to explain all the characteristics of mechano-sorption that are observed in the laboratory, summarized by Grossman [60] and Mårtensson [20].

The results of different studies can be contradictory to each other. As an example, it is not clear whether adsorption is leading to MS decrease or increase [20]. The mismatching observations are mainly due to their high dependency on the tested species and testing setups. As a consequence, there remain uncertainties in the modelling requirements given in Grossman [60] and Mårtensson [20] based on the observation summary. In addition, further experiments are required to clarify the uncertainties. Yet, these models provide important guidelines for model

developments and for model capability analysis.

Except for the primitive dashpot model, co-excitation model, and the sophisticated micro-stress redistribution model [50], the Kelvin-type model, generalized Maxwell model, and hydro-lock model are all capable of capturing the MS creep at desorption and adsorption, as well as the MS creep limit when the moisture oscillates within certain thresholds. The different MS creep rates that are observed in adsorption and desorption can be addressed by using a stress- or strain-dependent hydro-expansion element [18,47], which can be associated with all the three types of models. The generalized Maxwell model has stronger physical background among the three types and the non-linearity of MS with stress level has been considered in the generalized Maxwell models [29,61] by using non-linear dashpots. The potential of 3D application and incorporating orthotropic failure criteria was also studied [49]. Hydro-lock type model assumes viscoelastic nature of MS creep, and shows a good capability in describing the (++) effect and the partial recovery, which is taken into account by the higher creep of wetter wood [52]. Efforts in improving Kelvin-type models to mathematically describe further MS features can be found in wide ranges of studies, such as MS difference in compression and tension [22], partial MS recovery [30], time-dependent Poisson's ratio [44], association with damage mechanism [33] and plasticity [32], etc. Moreover, as most of the mechanical analogous models are only valid over the time span for which the parameters are calculated, a comparison of four models [20,41,61,62] and their accuracy in predicting the wood behavior under a load duration of 50 years can be found in the study of Schänzlin [13].

3. A generalized elastic-plastic viscoelastic MS model

3.1. Introduction

This work selected a Kelvin-type model [28] as the starting point for the developments. The model is extended to cover plasticity and further modifications are made primarily to the mechano-sorptive component. With the modification, the model is aimed to describe the following mechano-sorption features [20,60]:

- MS creep limit: MS creep happens along with moisture content cycles. When moisture content is cycling within a fixed threshold, the creep strain goes towards a limit value with a decreasing creep rate [2,35];
- Different MS creep rates under desorption and adsorption [20];
- Transcending creep: the effect of moisture content appears to be more pronounced for changes outside earlier attained threshold of moisture content, in comparison with the behaviour when the changes take place within the moisture limits that have been attained earlier [17,20];
- MS recovery:
- 1) the recovery of wood after unloading is similar to that for normal creep, but accelerated by moisture cycling [20];
- 2) experiments showed that a certain proportion of the developed MS creep does not recover, even if the load is removed and drying continues [16,45];
- 3) if unloading takes place at a relatively low moisture content, large recovery occurres when moisture content increases after the unloading point [1,17].

Moreover, under high compression load, wood develops a strain that is not immediately recoverable after removing the load but partially recoverable after certain moisture cycles. Here, this strain is considered as plastic strain plus a partially recoverable MS strain and is taken into account by a plastic component and the MS components in the model, respectively. Furthermore, the anisotropic Hill yielding criterion [63] is assumed in this work, as wood exhibits brittle behavior under tension and ductile behavior under compression.

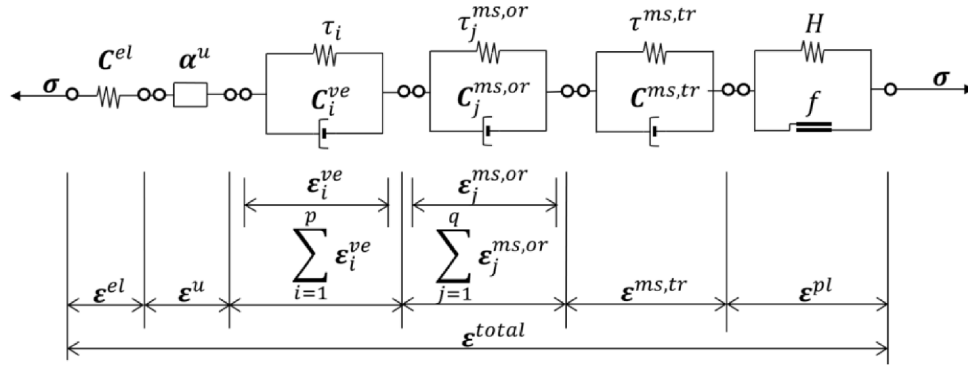As a result, an advanced 3D model is created taking into account

Fig. 1. Schematic illustration of the generalized constitutive model.

orthotropy, elastic-plasticity, hydro-expansion, elastic-plasticity, visco-elasticity, and mechano-sorption.

As can be seen in Fig. 1, a serial type of model is used, where the total strain tensor ε^{total} is the sum of different strain components, i.e. elastic (ε^{el}), hydro-expansion (ε^u), viscoelastic (ε^{ve}), ordinary and transcending mechano-sorptive ($\varepsilon^{ms,or}$ and $\varepsilon^{ms,tr}$), and plastic (ε^{pl}) ones:

$$\boldsymbol{\varepsilon}^{total} = \boldsymbol{\varepsilon}^{el} + \boldsymbol{\varepsilon}^u + \sum_{i=1}^{p}\boldsymbol{\varepsilon}_i^{ve} + \left(\sum_{j=1}^{q}\boldsymbol{\varepsilon}_j^{ms,or} + \boldsymbol{\varepsilon}^{ms,tr}\right) + \boldsymbol{\varepsilon}^{pl} \tag{3.1.1}$$

From a thermodynamic perspective [30], the Helmholtz free energy (ψ) is defined as:

$$\psi\left(T, u, \boldsymbol{\varepsilon}^{total}, \boldsymbol{\varepsilon}^u, \boldsymbol{\varepsilon}_i^{ve}, \boldsymbol{\varepsilon}_j^{ms,or}, \boldsymbol{\varepsilon}^{ms,tr}, \alpha\right) =$$
$$\psi(T, u) + \psi^{el}\left(\boldsymbol{\varepsilon}^{el}\right) + \psi^{ve}\left(\boldsymbol{\varepsilon}_i^{ve}\right) + \psi^{ms,or}\left(\boldsymbol{\varepsilon}_j^{ms,or}\right) + \psi^{ms,tr}(\boldsymbol{\varepsilon}^{ms,tr}) + \psi^{pl}(\alpha) \tag{3.1.2}$$

where ψ^{el}, ψ^{ve}, $\psi^{ms,or}$, $\psi^{ms,tr}$ are the energy stored in the elastic, visco-elastic, mechano-sorptive elements, and ψ^{pl} represents the plastic dissipation (isotropic hardening is considered):

$$\psi^{el}\left(\boldsymbol{\varepsilon}^{el}\right) = \frac{1}{2}\left(\boldsymbol{\varepsilon}^{total} - \boldsymbol{\varepsilon}^u - \sum_{i=1}^{p}\boldsymbol{\varepsilon}_i^{ve} - \sum_{j=1}^{q}\boldsymbol{\varepsilon}_j^{ms,or} - \boldsymbol{\varepsilon}^{ms,tr} - \boldsymbol{\varepsilon}^{pl}\right)$$
$$: \boldsymbol{C}_{(u)}^{el} : \left(\boldsymbol{\varepsilon}^{total} - \boldsymbol{\varepsilon}^u - \sum_{i=1}^{p}\boldsymbol{\varepsilon}_i^{ve} - \sum_{j=1}^{q}\boldsymbol{\varepsilon}_j^{ms,or} - \boldsymbol{\varepsilon}^{ms,tr} - \boldsymbol{\varepsilon}^{pl}\right);$$

$$\psi^{ve}\left(\boldsymbol{\varepsilon}_i^{ve}\right) = \frac{1}{2}\sum_{i=1}^{p}\boldsymbol{\varepsilon}_i^{ve} : \boldsymbol{C}_{i(u)}^{ve} : \boldsymbol{\varepsilon}_i^{ve};$$

$$\psi^{pl}(\alpha) = \frac{1}{2}q\alpha^2;$$

$$\psi^{ms,or}\left(\boldsymbol{\varepsilon}_j^{ms}\right) = \frac{1}{2}\sum_{j=1}^{q}\boldsymbol{\varepsilon}_j^{ms,or} : \boldsymbol{C}_{j(u)}^{ms,or} : \boldsymbol{\varepsilon}_j^{ms,or}; \psi^{ms,tr}(\boldsymbol{\varepsilon}^{ms,tr}) = \frac{1}{2}\boldsymbol{\varepsilon}^{ms,tr} : \boldsymbol{C}_{(u)}^{ms,tr} : \boldsymbol{\varepsilon}^{ms,tr} \tag{3.1.3}$$

The above parameters $\boldsymbol{C}_{i(u)}^{ve}$, q, α, $\boldsymbol{C}_{j(u)}^{ms,or}$, $\boldsymbol{C}_{(u)}^{ms,tr}$ will be explained in the following subsections. As the temperature is assumed to be constant in the present work, the thermal energy $\psi(T,u)$ remains constant. The derivation of the total stress tensor as well as the derivation of each partial stress tensor from the above thermodynamic equations will be given in the following subsections.

3.2. Elastic strain

The main constitutive equation of the model is obtained by differentiating the free energy with respect to the total strain tensor and this provides the total stress tensor:

$$\sigma = \frac{\partial\psi}{\partial\varepsilon^{total}} = C_{(u)}^{el} : \varepsilon^{el} \tag{3.2.1}$$

In case of orthotropic elasticity, the elastic compliance tensor $\boldsymbol{C}_{(u)}^{el\ -1}$ is:

$$\boldsymbol{C}_{(u)}^{el\ -1} = \begin{bmatrix} \dfrac{1}{E_R} & \dfrac{-v_{TR}}{E_T} & \dfrac{-v_{LR}}{E_L} & 0 & 0 & 0 \\[2mm] \dfrac{-v_{TR}}{E_T} & \dfrac{1}{E_T} & \dfrac{-v_{LT}}{E_L} & 0 & 0 & 0 \\[2mm] \dfrac{-v_{LR}}{E_L} & \dfrac{-v_{LT}}{E_L} & \dfrac{1}{E_L} & 0 & 0 & 0 \\[2mm] 0 & 0 & 0 & \dfrac{1}{G_{RT}} & 0 & 0 \\[2mm] 0 & 0 & 0 & 0 & \dfrac{1}{G_{RL}} & 0 \\[2mm] 0 & 0 & 0 & 0 & 0 & \dfrac{1}{G_{TL}} \end{bmatrix} \tag{3.2.2}$$

The elastic compliance tensor $\boldsymbol{C}_{(u)}^{el\ -1}$ is moisture dependent. Therefore all the engineering constants (E_i and G_{ij}) can be expressed as a function of the moisture content (u):

$$E_{i(u)} = E_{i,ref} + b_i *\left(u - u_{ref}\right) \ with \ i = R, T, L$$
$$G_{ij(u)} = G_{ij,ref} + b_{ij} *\left(u - u_{ref}\right) \ with \ i, j = R, T, L; i \neq j \tag{3.2.3}$$

where $E_{i,ref}$ and $G_{ij,ref}$ are the values at reference moisture content u_{ref}. Hence, the rate form of elastic strain can be presented as:

$$\dot{\boldsymbol{\varepsilon}}^{el} = \dot{\boldsymbol{\varepsilon}}^{el,\Delta u} + \dot{\boldsymbol{\varepsilon}}^{el,\Delta\sigma} = \dot{\boldsymbol{C}}_{(u)}^{el\ -1} : \boldsymbol{\sigma}_n + \boldsymbol{C}_n^{el-1} : \dot{\boldsymbol{\sigma}} \tag{3.2.4}$$

The incremental elastic strain reads:

$$\Delta\boldsymbol{\varepsilon}_{n+1}^{el} = \Delta\boldsymbol{\varepsilon}_{n+1}^{el,\Delta\sigma} + \Delta\boldsymbol{\varepsilon}_{n+1}^{el,\Delta u} = \Delta\boldsymbol{C}_{n+1}^{el\ -1} : \boldsymbol{\sigma}_n + \boldsymbol{C}_n^{el-1} : \Delta\boldsymbol{\sigma}_{n+1} \tag{3.2.5}$$

3.3. Hydro-expansion

Hydro-expansion takes the following mathematical rate form:

$$\dot{\boldsymbol{\varepsilon}}^u = \boldsymbol{\alpha}^u\left(1 - \boldsymbol{\beta}^u\boldsymbol{\varepsilon}^{mech}\right)\dot{u} \tag{3.3.1}$$

where $\boldsymbol{\alpha}^u = [\alpha_R^u, \alpha_T^u, \alpha_L^u, 0, 0, 0]$ includes the hydro-expansion coefficients, $\boldsymbol{\varepsilon}^{mech} = \boldsymbol{\varepsilon}^{total} - \boldsymbol{\varepsilon}^u$ is the mechanical strain, and $\boldsymbol{\beta}^u = [\beta_R^u, \beta_T^u, \beta_L^u, 0, 0, 0]$ describes the strain-dependency of hydro-expansion, which is proven in the studies of Hunt and Shelton [35]. Such application can explain partially the difference of MS creep rate during subsequent sorptions and desorptions.

3.4. Viscoelastic strain

Viscoelasticity was modeled by a serial association of Kelvin-Voigt elements. By taking the derivative of the free energy function with respect to the element-wise viscoelastic strain, the driving stress for the ith viscoelastic Kelvin–Voigt element can be obtained:

$$\sigma_i^{ve} = -\frac{\partial \psi}{\partial \varepsilon_i^{ve}} = C_{(u)}^{el} : \varepsilon^{el} - C_{i(u)}^{ve} : \varepsilon_i^{ve} = \sigma - C_{i(u)}^{ve} : \varepsilon_i^{ve} \tag{3.4.1}$$

where the viscoelastic compliance tensor $C_{i(u)}^{ve\ -1}$ is assumed to be proportional to the elastic tensor with a moisture dependent ratio J_i^{ve}:

$$C_{i(u)}^{ve\ -1} = J_i^{ve} C_{(u)}^{el\ -1} \tag{3.4.2}$$

$$J_i^{ve} = J_{i,ref}^{ve} + \beta_i^{ve} (u - u_{ref}) \tag{3.4.3}$$

Accordingly, the rate of the viscoelastic strain can be derived from the viscoelastic stress:

$$\dot{\varepsilon}_i^{ve} = \frac{1}{\tau_i} C_{i(u)}^{ve\ -1} : \sigma_i^{ve} \tag{3.4.4}$$

By inserting equation (3.4.4) into equation (3.4.1), the rate form of the governing equation for i^{th} Kelvin-Voigt element can be obtained:

$$\dot{\varepsilon}_i^{ve} + \frac{1}{\tau_i} \varepsilon_i^{ve} = \frac{1}{\tau_i} C_{i(u)}^{ve\ -1} : \sigma_{(t)} \tag{3.4.5}$$

where τ_i represents the retardation time of the ith Kelvin element. Using Laplace transformation, the heredity integral form of the stress driven problem can be obtained as:

$$\varepsilon_i^{ve}(t) = \int_0^t e^{\left(\frac{\zeta-t}{\tau_i}\right)} \frac{C_{i(u)}^{ve\ -1} : \sigma_{(\zeta)}}{\tau_i} d\zeta = \int_0^t (1 - e^{\left(\frac{\zeta-t}{\tau_i}\right)}) \dot{\sigma}_{(\zeta)} d\zeta \tag{3.4.6}$$

and the incremental strain development can be described as [30]:

$$\varepsilon_{i,n+1}^{ve} = e^{\frac{-\Delta t}{\tau_i}} \varepsilon_{i,n}^{ve} + \int_{t_n}^{t_{n+1}} \frac{C_{i(u)}^{ve\ -1} : \sigma_{(\zeta)}}{\tau_i} e^{\left(-\frac{t_{n+1}-\zeta}{\tau_i}\right)} d\zeta \tag{3.4.7}$$

Using integration by part and assuming at each time increment $\Delta t = t_{n+1} - t_n$ that:

$$\frac{\partial \left(C_{i(u)}^{ve\ -1} : \sigma_{(\zeta)}\right)}{\partial t} = \frac{\left(C_{i(u_{n+1})}^{ve\ -1} : \sigma_{(n+1)} - C_{i(u_n)}^{ve\ -1} : \sigma_{(n)}\right)}{\Delta t} = constant \tag{3.4.8}$$

the following equations can be derived:

$$\Delta \varepsilon_{i,n+1}^{ve} = \varepsilon_{i,n}^{ve,i} \left[exp\left(\frac{-\Delta t}{\tau_i}\right) - 1 \right] + T_{i,n}^{ve} C_{i(u_n)^{-1}}^{ve} : \sigma_n + T_{i,n+1}^{ve} C_{i(u_{n+1})^{-1}}^{ve} : \sigma_{n+1}$$

$$where\ T_{i,n+1}^{ve} = 1 - \frac{1 - e^{\frac{-\Delta t}{\tau_i}}}{\Delta t / \tau_i},\ T_{i,n}^{ve} = 1 - e^{\frac{-\Delta t}{\tau_i}} - T_{i,n+1}^{ve}$$

$$\tag{3.4.9}$$

3.5. Mechano-sorptive strain

As shown in Fig. 1, in the new construction of the MS model, the mechano-sorption is divided into two parts, namely the ordinary MS and the transcending MS. In terms of recovery, efforts have been made in addressing the partial recoverability of MS creep, such as the modified Kelvin-type models mentioned in Table 1 [18,28]. However, there remain some discrepancies between the simulation and experiment at the recovery phase in the work of Fortino et al. [28]. According to Ranta-Maunus [17], the MS recovery is defined to happen at the moment ç after unloading, such that the moisture content surpassing the moisture content at the unloading moment t^*, also called the critical moisture interval:

$$u(\varsigma). > u(t^*)\ for\ t^* < \varsigma < t \tag{3.5.1}$$

Although full-MS-recovery (which is not the case of wood) is assumed in the study of Ranta-Maunus [17], it provides an inspiratory way of addressing transcending mechano-sorptive creep. Similar approach can be found in the hydro-lock type of model [56], where strain is controlled by the minimum stiffness k_{min}, which is only updated, as after unloading point, when moisture content surpasses the critical moisture interval $u(t^*)$.

In this work, both ordinary and transcending part of MS are modelled using Kelvin-Voigt elements analogous to the viscoelastic Kelvin-Voigt elements. Instead of time increment Δt, the ordinary and transcending MS parts are driven by the moisture content increment Δu and the transcending moisture increment ΔU, respectively. The transcending moisture content U is defined as the maximum moisture content during each mechanical loading phase, as shown in Fig. 2.

Analogous to viscoelastic part, by taking the derivative of the free energy function with respect to the element-wise MS strain, the driving stress for the jth ordinary Kelvin–Voigt element and for the transcending Kelvin-Voigt element can be obtained:

$$\sigma_j^{ms,or} = -\frac{\partial \psi}{\partial \varepsilon_j^{ms,or}} = C_{(u)}^{el} : \varepsilon^{el} - C_{j(u)}^{ms,or} : \varepsilon_j^{ms,or} = \sigma - C_{j(u)}^{ms,or} : \varepsilon_j^{ms,or} \tag{3.5.2}$$

$$\sigma^{ms,tr} = -\frac{\partial \psi}{\partial \varepsilon^{ms,tr}} = C_{(u)}^{el} : \varepsilon^{el} - C_{(u)}^{ms,tr} : \varepsilon^{ms,tr} = \sigma - C_{(u)}^{ms,tr} : \varepsilon^{ms,tr} \tag{3.5.3}$$

where $C_{j(u)}^{ms,or}$ and $C_{(u)}^{ms,tr}$ stand for the ordinary and transcending mechano-sorptive stiffness tensors. Following the work of Fortino et al. [28], the $C_{j(u)}^{ms,or}$ can be calibrated based on the elastic engineering constants:
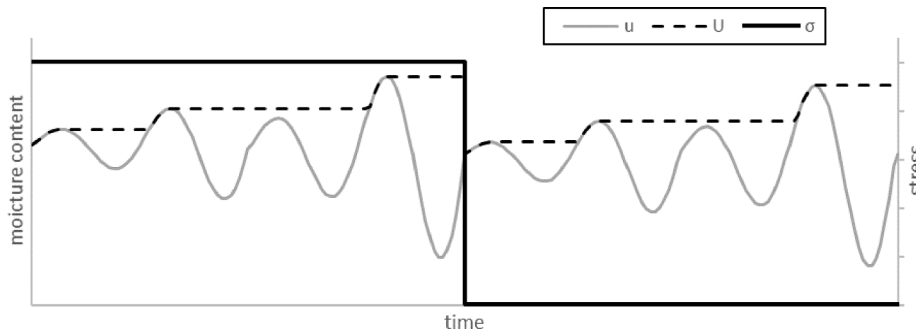

Fig. 2. Illustration of moisture content u and the transcending moisture content U

$$C_{j(u)}^{ms,or\,-1} = \begin{bmatrix} \dfrac{1}{E_R}\left(J_{j,T}^{ms}E_{T,\mathrm{ref}}\right) & \dfrac{-v_{TR}}{E_T}\left(J_{j,T}^{ms}E_{T,\mathrm{ref}}\right) & \dfrac{-v_{LR}}{E_L}\left(J_{j,T}^{ms}E_{T,\mathrm{ref}}\right) & 0 & 0 & 0 \\[2ex] \dfrac{-v_{TR}}{E_T}\left(J_{j,T}^{ms}E_{T,\mathrm{ref}}\right) & \dfrac{1}{E_T}\left(J_{j,T}^{ms}E_{T,\mathrm{ref}}\right) & \dfrac{-v_{LT}}{E_L}\left(J_{j,T}^{ms}E_{T,\mathrm{ref}}\right) & 0 & 0 & 0 \\[2ex] \dfrac{-v_{LR}}{E_L}\left(J_{j,T}^{ms}E_{T,\mathrm{ref}}\right) & \dfrac{-v_{LT}}{E_L}\left(J_{j,T}^{ms}E_{T,\mathrm{ref}}\right) & \dfrac{1}{E_L}\left(J_{j,L}^{ms}\right) & 0 & 0 & 0 \\[2ex] 0 & 0 & 0 & \dfrac{J_{j,T}^{ms}E_{T,\mathrm{ref}}}{G_{RT}} & 0 & 0 \\[2ex] 0 & 0 & 0 & 0 & \dfrac{J_{j,T}^{ms}E_{T,\mathrm{ref}}}{G_{RL}} & 0 \\[2ex] 0 & 0 & 0 & 0 & 0 & \dfrac{J_{j,T}^{ms}E_{T,\mathrm{ref}}}{G_{TL}} \end{bmatrix} \tag{3.5.4}$$

where $J_{j,L}^{ms}$ and $J_{j,T}^{ms}$ are constants, which take into account the different MS behaviors in longitudinal and transverse directions. For transcending compliance tensor, a uniform ratio $J^{ms,tr}$ is assumed for all directions as a simplification:

$$C_{(u)}^{ms,tr\,-1} = J^{ms,tr}C_{(u)}^{el\,\,-1} \tag{3.5.5}$$

According to equation (3.5.2) and (3.5.3), the rate of mechanosorptive strain of each Kelvin-Voigt element can be derived from the mechano-sorptive driving force:

$$\dot{\boldsymbol{\varepsilon}}_j^{ms,or} = \frac{|\dot{u}|}{\tau_j}\boldsymbol{C}_{j(u)}^{ms,or-1} : \boldsymbol{\sigma}_j ms, or \tag{3.5.6}$$

$$\dot{\boldsymbol{\varepsilon}}^{ms,tr} = \frac{|\dot{U}|}{\tau_{tr}}\boldsymbol{C}_{(u)}^{ms,tr-1} : \boldsymbol{\sigma}^{ms,tr} \tag{3.5.7}$$

where τ_j and τ_{tr} are the characteristic moisture content for j^{th} ordinary MS element and transcending MS element, respectively. They are analogous to the characteristic retardation time for the viscoelastic element. Subsequently, the rate form of the governing equation for MS element is:

$$\dot{\boldsymbol{\varepsilon}}_j^{ms,or} + \frac{|\dot{u}|}{\tau_j}\boldsymbol{\varepsilon}_j^{ms,or} = \frac{|\dot{u}|}{\tau_j}\boldsymbol{C}_{j(u)}^{ms,or-1} : \boldsymbol{\sigma}_{(t)} \tag{3.5.8}$$

$$\dot{\boldsymbol{\varepsilon}}^{ms,tr} + \frac{|\dot{U}|}{\tau_{tr}}\boldsymbol{\varepsilon}^{ms,tr} = \frac{|\dot{U}|}{\tau_{tr}}\boldsymbol{C}_{(u)}^{ms,tr-1} : \boldsymbol{\sigma}_{(t)} \tag{3.5.9}$$

Using the same approach for viscoelastic part, the final strain increment of each MS element can be derived:

$$\Delta\boldsymbol{\varepsilon}_{j,n+1}^{ms,or} = \boldsymbol{\varepsilon}_{j,n}^{ms,or}\left[\exp\left(\frac{-|\Delta u|}{\tau_j}\right) - 1\right] + \mathbb{T}_{j,n}^{ms,or}\boldsymbol{C}_{j(u_n)}^{ms,or-1} : \boldsymbol{\sigma}_n + \mathbb{T}_{j,n+1}^{ms,or}\boldsymbol{C}_{j(u_{n+1})}^{ms,or\,\,-1} : \boldsymbol{\sigma}_{n+1}$$

$$where\ \mathbb{T}_{j,n+1}^{ms,or} = 1 - \frac{1 - e^{\frac{-|\Delta u|}{\tau_j}}}{\frac{|\Delta u|}{\tau_j}}, \ \mathbb{T}_{j,n}^{ms,or} = 1 - e^{\frac{-|\Delta u|}{\tau_j}} - \mathbb{T}_{j,n+1}^{ms,or} \tag{3.5.10}$$

$$\Delta\boldsymbol{\varepsilon}_{n+1}^{ms,tr} = \boldsymbol{\varepsilon}_n^{ms,tr}\left[\exp\left(\frac{-|\Delta U|}{\tau_{tr}}\right)\right] + \mathbb{T}_n^{ms,tr}\boldsymbol{C}_{(u_n)}^{ms,tr-1} : \boldsymbol{\sigma}_n + \mathbb{T}_{n+1}^{ms,tr}\boldsymbol{C}_{(u_{n+1})}^{ms,tr\,\,-1} : \boldsymbol{\sigma}_{n+1}$$

$$where\ \mathbb{T}_{n+1}^{ms,tr} = 1 - \frac{1 - e^{\frac{-|\Delta U|}{\tau_{tr}}}}{\frac{|\Delta U|}{\tau_{tr}}}, \ \mathbb{T}_n^{ms,tr} = 1 - e^{\frac{-|\Delta U|}{\tau_{tr}}} - \mathbb{T}_{n+1}^{ms,tr} \tag{3.5.11}$$

3.6. Plastic strain

As an extension of von Mises criterion, which is used for isotropic materials, Hill yielding criterion [63] covers the anisotropy in plasticity, which is proven to be suitable for some wood species under compression [64]. However, wood exhibits more complicated features when approaching the limit state, such as the different response under tensile and compressive loads. Accordingly, further developments have been made [65,66], including using Hoffman type function [65] or multi-surface plastic model [66], associating with Tsai-Hill fracture criterion [67] or with damage mechanism [68], etc. However, calibrating the model for exact plastic behavior of wood is not the main focus of this work. Hence, Hill yielding criterion [63] with isotropic exponential hardening law is adopted, to show the approach of combining the above mentioned time- and moisture-dependent behaviors of wood with plasticity. Hill yielding criterion [63] can be expressed as:

$$f_{(\boldsymbol{\sigma},\alpha,u)} = \sqrt{\boldsymbol{\sigma} : \boldsymbol{A}_{(u)} : \boldsymbol{\sigma}} - q_{(\alpha,u)}^{pl} \tag{3.6.1}$$

where $q_{(\alpha,u)}^{pl}$ represents the hardening law and $\boldsymbol{A}_{(u)}$ can be calculated as:

$$\boldsymbol{A}_{(u)} = \begin{bmatrix} H_{(u)} + G_{(u)} & -H_{(u)} & -G_{(u)} & 0 & 0 & 0 \\ -H_{(u)} & F_{(u)} + H_{(u)} & -F_{(u)} & 0 & 0 & 0 \\ -G_{(u)} & -F_{(u)} & F_{(u)} + G_{(u)} & 0 & 0 & 0 \\ 0 & 0 & 0 & 2N_{(u)} & 0 & 0 \\ 0 & 0 & 0 & 0 & 2M_{(u)} & 0 \\ 0 & 0 & 0 & 0 & 0 & 2L_{(u)} \end{bmatrix} \tag{3.6.2}$$

The parameters that are related to the material properties F, G, H, L, M, and N are given as:

$$F_{(u)} = \frac{1}{2}\left(-\frac{f_0^2}{f_{R(u)}^2} + \frac{f_0^2}{f_{T(u)}^2} + \frac{f_0^2}{f_{L(u)}^2}\right), \quad N_{(u)} = \frac{f_0^2}{2f_{TL(u)}^2}$$

$$G_{(u)} = \frac{1}{2}\left(\frac{f_0^2}{f_{R(u)}^2} - \frac{f_0^2}{f_{T(u)}^2} + \frac{f_0^2}{f_{L(u)}^2}\right), \quad M_{(u)} = \frac{f_0^2}{2f_{RL(u)}^2}$$

$$H_{(u)} = \frac{1}{2}\left(\frac{f_0^2}{f_{R(u)}^2} + \frac{f_0^2}{f_{T(u)}^2} - \frac{f_0^2}{f_{L(u)}^2}\right), \quad L_{(u)} = \frac{f_0^2}{2f_{RT(u)}^2} \qquad (3.6.3)$$

where $f_0 = f_{R(u)}, f_{T(u)}$, and $f_{L(u)}$ are yielding tension/compression strengths and $f_{RT(u)}, f_{TL(u)}$, and $f_{TL(u)}$ are the yielding shear strengths. The internal variable α is equal to the equivalent plastic strain $\bar{\varepsilon}^p$:

$$\alpha = \bar{\varepsilon}^p \qquad (3.6.4)$$

The exponential isotropic hardening is used:

$$q_{(\alpha,u)}^{pl} = Q\left(1 - e^{-b\alpha}\right) + f_0 \qquad (3.6.5)$$

where b and Q are shape parameters. Associated flow rule is assumed:

$$\dot{\boldsymbol{\varepsilon}}^{pl} = \dot{\gamma}\frac{\partial f_{(\sigma,\alpha,u)}}{\partial \boldsymbol{\sigma}} \qquad (3.6.6)$$

where $\dot{\gamma}$ is the plastic flow parameter. According to the backward Euler method, the basic plastic equations in the incremental form read:

$$\boldsymbol{\varepsilon}_{n+1}^{pl} = \boldsymbol{\varepsilon}_n^{pl} + \Delta\gamma\partial_\sigma f_{n+1} \qquad (3.6.7)$$

$$\alpha_{n+1} = \alpha_n + \Delta\gamma\partial_q f_{n+1} \qquad (3.6.8)$$

$$\boldsymbol{\sigma}_{n+1} = \boldsymbol{C}_{n+1}^{el} : \left(\boldsymbol{\varepsilon}_{n+1}^{\Delta\sigma} - \sum_i \boldsymbol{\varepsilon}_{i,n+1}^{ve} - \sum_j \boldsymbol{\varepsilon}_{j,n+1}^{ms,or} - \boldsymbol{\varepsilon}_{n+1}^{ms,tr} - \Delta\boldsymbol{\varepsilon}_{n+1}^{pl}\right) \qquad (3.6.9)$$

$$f_{n+1}(\boldsymbol{\sigma}, \alpha, u) = f_{n+1}(\Delta\gamma, u) = 0 \qquad (3.6.10)$$

3.7. Moisture transfer model

In the present work, a semi-coupled moisture-stress analysis is performed to analyze the wood behaviour under the interaction of mechanical load and moisture variation. Wood is assumed to follow Fick's law for moisture transfer and the temperature is considered to be constant.

$$\left.\frac{\partial u}{\partial t}\right|_\Omega = \nabla \bullet (\boldsymbol{D} \bullet \nabla \mathrm{u}) \qquad (3.7.1)$$

where the diffusion coefficient $\boldsymbol{D}$ is:

$$\boldsymbol{D} = diag[D_R \quad D_T \quad D_L] \qquad (3.7.2)$$

The moisture flow at the wood surface is expressed by using the following equation [69,70] :

$$\frac{q_n}{\rho} = S_u(u_{air} - u_{surf}) \qquad (3.7.3)$$

where q_n represents the moisture flow across the boundary, S_u is the coefficient of surface emission, u_{surf} is the moisture content of the wood surface and u_{air} the equilibrium moisture content of wood corresponding to the relative humidity (RH).

4. Algorithm

In this work the algorithm for moisture induced stress update is implemented in the framework of user subroutine UMAT of Abaqus. Before entering the mechanical analysis, moisture increment Δu_{n+1} for the current time step t_{n+1} is obtained from the semi-coupled moisture transfer analysis. The total strain increment $\Delta\boldsymbol{\varepsilon}_{n+1}^{total}$ (DSTRAN in UMAT) is calculated through the tangent matrix $\boldsymbol{C}_n^T$ (DDSDDE in UMAT) from the last time step. The information of stress and strain components of the last
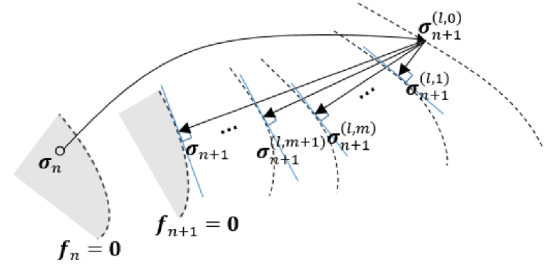

Fig. 3. Illustration of closest point projection approach algorithm [71]

time step are stored in the variable STRESS and State Variables.

The flow diagram in Fig. 4 gives an overview of the algorithm that is implemented into UMAT. In order to calculate the stress-driven strain increment, a time- and moisture-dependent creep loop (abbreviated as l_LOOP) and a plastic loop (abbreviated as m_LOOP) are designed. Before entering the loops, the strain increments driven solely by moisture change are updated and used to obtain the trail values according to equations (4.1-4.3). The m_LOOP is designed as a plastic-corrector subroutine consisting of equation (4.4-4.18) and is implemented into the l_LOOP. After receiving the corrected stress increment value, the viscoelastic and mechano-sorptive strains are updated in the l_LOOP according to equations (4.19-4.30). The corresponding operator tensor is calculated by equation (4.25).

The total strain ($\Delta\boldsymbol{\varepsilon}_{n+1}^{total}$) can be decomposed into two parts:

- A moisture-driven strain ($\Delta\boldsymbol{\varepsilon}_{n+1}^{\Delta u}$), which can be calculated based on the Δu_{n+1} and $\boldsymbol{\sigma}_n$ of the previous increment. It is composed of the hydro-expansion ($\Delta\boldsymbol{\varepsilon}_{n+1}^u$) and the moisture-driven part of elastic strain ($\Delta\boldsymbol{\varepsilon}_{n+1}^{el,\Delta u}$);

$$\Delta\boldsymbol{\varepsilon}_{n+1}^{\Delta u} = \Delta\boldsymbol{\varepsilon}_{n+1}^u + \Delta\boldsymbol{\varepsilon}_{n+1}^{el,\Delta u} \qquad (4.1)$$

- A stress-driven strain ($\Delta\boldsymbol{\varepsilon}_{n+1}^{\Delta\sigma}$), which is a function of the stress increment $\Delta\sigma_{n+1}$. It is composed of the stress-driven part of elastic strain ($\Delta\boldsymbol{\varepsilon}_{n+1}^{el,\Delta\sigma}$), the viscoelastic strain ($\sum_i \Delta\boldsymbol{\varepsilon}_{i,n+1}^{ve}$), mechano-sorptive strains ($\sum_j \Delta\boldsymbol{\varepsilon}_{j,n+1}^{ms,or}$ and $\Delta\boldsymbol{\varepsilon}_{n+1}^{ms,tr}$) , and plastic strain ($\Delta\boldsymbol{\varepsilon}_{n+1}^{pl}$).

$$\Delta\boldsymbol{\varepsilon}_{n+1}^{\Delta\sigma} = \Delta\boldsymbol{\varepsilon}_{n+1}^{el,\Delta\sigma} + \sum_i \Delta\boldsymbol{\varepsilon}_{i,n+1}^{ve} + \sum_j \Delta\boldsymbol{\varepsilon}_{j,n+1}^{ms,or} + \Delta\boldsymbol{\varepsilon}_{n+1}^{ms,tr} + \Delta\boldsymbol{\varepsilon}_{n+1}^{pl} \qquad (4.2)$$

At the beginning of each increment, based on the input values(i.e. Δu_{n+1} and stress information of last time step σ_n), all the moisture related parameters including $\boldsymbol{C}_{n+1}^{el}$, $\boldsymbol{C}_i^{ve}$, $\boldsymbol{C}_j^{ms,or}$, $\boldsymbol{C}_{n+1}^{ms,tr}$, and plastic parameters $A_{(u)}$ can be updated, and the moisture-driven strain ($\Delta\boldsymbol{\varepsilon}_{n+1}^{\Delta u}$) can be calculated.

For time step t_{n+1}, the possible development of irrecoverable deformation by plastic strain is examined. For this purpose, a two-step return-mapping algorithm known as plastic corrector based on the general closest point projection approach algorithm [71] is adopted (Fig. 3).

As for the trial status, the time step is first assumed to be elastic, which means upon entering the l_LOOP, i.e.$l = 0$:

$$\Delta\boldsymbol{\varepsilon}_{i,n+1}^{ve(l=0)} = 0, \quad \Delta\boldsymbol{\varepsilon}_{j,n+1}^{ms(l=0)} = 0, \quad \Delta\boldsymbol{\varepsilon}_{n+1}^{ms,tr(l=0)} = 0 \qquad (4.3)$$

and upon entering the m_LOOP, i.e. $m = 0$:

$$\boldsymbol{\varepsilon}_{n+1}^{pl(l,m=0)} = \boldsymbol{\varepsilon}_n^{pl}, \quad \alpha_{n+1}^{(l,m=0)} = \alpha_n, \quad \Delta\gamma_{n+1}^{(l,m=0)} = 0 \qquad (4.4)$$

$$\Delta\sigma_{n+1}^{(l,m=0)} = \boldsymbol{C}_{n+1}^{el} : \Delta\boldsymbol{\varepsilon}_{n+1}^{ep(l)} \qquad (4.5)$$

where $\Delta\boldsymbol{\varepsilon}_{n+1}^{ep}$ is the sum of elastic and plastic strains. For the initial status, the following equation is valid:
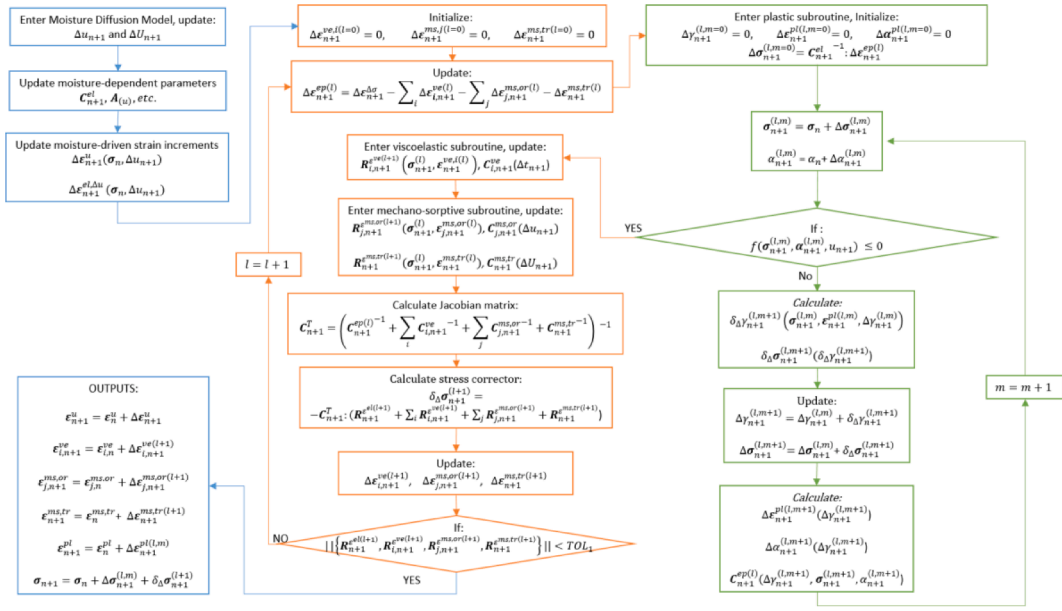
Fig. 4. Flow diagram of UMAT.

$$\Delta\boldsymbol{\varepsilon}_{n+1}^{ep(l,m=0)} = \Delta\boldsymbol{\varepsilon}_{n+1}^{\Delta\sigma} - \sum_i \Delta\boldsymbol{\varepsilon}_{i,n+1}^{ve(l)} - \sum_j \Delta\boldsymbol{\varepsilon}_{j,n+1}^{ms,or(l)} - \Delta\boldsymbol{\varepsilon}_{n+1}^{ms,tr(l)} \tag{4.6}$$

According to closest point projection approach algorithm, the position of corresponding trial stress $\Delta\boldsymbol{\sigma}_{n+1}^{(l,m)}$ with respect to the implemented yield surface is checked according to the yield function $f_{(\sigma,\alpha,u)}$ (3.6.1). If $f\left(\boldsymbol{\sigma}_{n+1}^{(l,m)}, \alpha_{n+1}^{(l,m)}, u\right) \leq 0$, the deformation is purely elastic and the trial value remains. If $f\left(\boldsymbol{\sigma}_{n+1}^{(l,m)}, \alpha_{n+1}^{(l,m)}, u\right) > 0$, plastic loading is the case and the trial state of stress $\Delta\boldsymbol{\sigma}_{n+1}^{(l,m)}$ calculated from the trial elastic strain needs to be projected onto the current yield surface.

According to equation (3.6.10), the first element of Taylor series expansion at point $\Delta\gamma_{n+1}^{(l,m)}$ takes zero:

$$0 = f_{n+1}^{(l,m+1)} = f_{n+1}^{(l,m)} + \delta_{\Delta\gamma}^{(l,m+1)} \partial_{\Delta\gamma} f_{n+1}^{(l,m)} \tag{4.7}$$

where $\delta_{\Delta\gamma}^{(l,m+1)}$ is the corrected value for the consistency parameter $\Delta\gamma_{n+1}^{(l,m)}$ at increment m. According to equations (3.6.7-3.6.9), the following euqation can be derived:

$$\delta_{\Delta\gamma}^{(l,m+1)} = \frac{f_{n+1}^{(l,m)}}{\partial_{\alpha} f_{n+1}^{(l,m)} : \boldsymbol{E}_{n+1}^{(l,m)} : \partial_{\alpha} f_{n+1}^{(l,m)} - \partial_{\alpha} f_{n+1}^{(l,m)}}$$

$$where \quad \boldsymbol{E}_{n+1}^{(l,m)} = \left(\boldsymbol{C}_{n+1}^{el}{}^{-1} + \Delta\gamma_{n+1}^{(l,m)} \partial_{\sigma}^2 f_{n+1}^{(l,m)}\right)^{-1} \tag{4.8}$$

Consequently, the stress $\boldsymbol{\sigma}_{n+1}^{(l,m)}$ needs to be updated by:

$$\delta_{\Delta}\boldsymbol{\sigma}_{n+1}^{(l,m+1)} = -\delta_{\Delta\gamma}^{(l,m+1)} \boldsymbol{E}_{n+1}^{(l,m)} : \partial_{\alpha} f_{n+1}^{(l,m)} \tag{4.9}$$

Hence, the state variables can be updated as:

$$\Delta\gamma_{n+1}^{(l,m+1)} = \Delta\gamma_{n+1}^{(l,m)} + \delta_{\Delta\gamma}^{(l,m+1)} \tag{4.10}$$

$$\Delta\boldsymbol{\sigma}_{n+1}^{(l,m+1)} = \Delta\boldsymbol{\sigma}_{n+1}^{(l,m)} + \delta_{\Delta}\boldsymbol{\sigma}_{n+1}^{(l,m+1)} \tag{4.11}$$

$$\boldsymbol{\varepsilon}_{n+1}^{pl(l,m+1)} = \boldsymbol{\varepsilon}_n^{pl} - \boldsymbol{C}_{n+1}^{el}{}^{-1} \delta_{\Delta}\boldsymbol{\sigma}_{n+1}^{(l,m)} \tag{4.12}$$

$$\alpha_{n+1}^{(l,m+1)} = \alpha_{n+1}^{(l,m)} + \delta_{\Delta\gamma}^{(l,m+1)} \tag{4.13}$$

Finally, the updated yielding function and residual parameters can be calculated as:

$$f_{n+1}^{(l,m+1)} = f_{\left(\boldsymbol{\sigma}_{n+1}^{(l,m+1)}, \alpha_{n+1}^{(l,m+1)}, u_{n+1}\right)} \tag{4.14}$$

$$\boldsymbol{R}_{n+1}^{\varepsilon pl} = -\boldsymbol{\varepsilon}_{n+1}^{pl(l,m+1)} + \boldsymbol{\varepsilon}_n^{pl} + \Delta\gamma_{n+1}^{(l,m+1)} \partial_{\alpha} f_{n+1}^{(l,m+1)} \tag{4.15}$$

$$R_{n+1}^{\alpha} = -\alpha_{n+1}^{(l,m+1)} + \alpha_n + \Delta\gamma_{n+1}^{(l,m+1)} \partial_{\alpha} f_{n+1}^{(l,m+1)} \tag{4.16}$$

The plastic iteration (m_LOOP) is repeated until $f_{n+1}^{(l,m+1)} \leq 0$ and until the residual parameters $\left\|\boldsymbol{R}_{n+1}^{\varepsilon pl}\right\| \leq TOL1$ and $\left|R_{n+1}^{\alpha}\right| \leq TOL2$.

The final elastic–plastic compliance matrix can be calculated as [71]:

$$\boldsymbol{C}_{n+1}^{ep(l)} = \boldsymbol{E}_{n+1} - \frac{(\boldsymbol{E}_{n+1} : \partial_{\alpha} f_{n+1}^{(l,m+1)}) \otimes (\partial_{\alpha} f_{n+1}^{(l,m+1)} : \boldsymbol{E}_{n+1})}{\partial_{\alpha} f_{n+1}^{(l,m+1)} : \boldsymbol{E}_{n+1} : \partial_{\alpha} f_{n+1}^{(l,m+1)} - \partial_{\alpha} f_{n+1}^{(l,m+1)}} \tag{4.17}$$

Using the resultant stress increment from the end of m_LOOP, the updated stress for l_LOOP can be updated as:

$$\boldsymbol{\sigma}_{n+1}^{(l)} = \boldsymbol{\sigma}_n + \Delta\boldsymbol{\sigma}_{n+1}^{(l,m+1)} \tag{4.18}$$

Correspondingly, the increment of elastic ($\Delta\boldsymbol{\varepsilon}_{n+1}^{el(l+1)}$), viscoelastic ($\Delta\boldsymbol{\varepsilon}_{i,n+1}^{ve(l+1)}$), and mechano-sorptive ($\Delta\boldsymbol{\varepsilon}_{j,n+1}^{ms,or(l+1)}$ and $\Delta\boldsymbol{\varepsilon}_{n+1}^{ms,tr(l+1)}$) strains can be calculated according to equations (3.2.5), (4.9), and (3.5.10-3.5.11). However, the sum of all the updated strain components in the current increment are no longer in equilibrium with the $\Delta\boldsymbol{\varepsilon}_{n+1}^{total}$ assigned for this time increment. The difference can be expressed by residual parameters:

$$\boldsymbol{R}_{n+1}^{\varepsilon(l+1)} = \left\{\boldsymbol{R}_{n+1}^{\varepsilon el(l+1)}, \boldsymbol{R}_{i,n+1}^{\varepsilon ve(l+1)}, \boldsymbol{R}_{j,n+1}^{\varepsilon ms,or(l+1)}, \boldsymbol{R}_{n+1}^{\varepsilon ms,tr(l+1)}\right\}^T \tag{4.19}$$

$$\boldsymbol{R}_{n+1}^{\varepsilon el(l+1)} = \boldsymbol{C}_{n+1}^{el}{}^{-1} : \boldsymbol{\sigma}_{n+1}^{(l)} - \left(\boldsymbol{\varepsilon}_{n+1}^{\Delta\sigma} - \boldsymbol{\varepsilon}_{n+1}^{pl(l)} - \sum_i \boldsymbol{\varepsilon}_{n+1}^{ve,i(l)} - \sum_j \boldsymbol{\varepsilon}_{n+1}^{ms,j(l)}\right) \tag{4.20}$$

$$\boldsymbol{R}_{i,n+1}^{\varepsilon ve(l+1)} = \left[\boldsymbol{\varepsilon}_{i,n}^{ve} \exp\left(\frac{-\Delta t}{\tau_i}\right) + \mathbb{T}_{i,n}^{ve} \boldsymbol{C}_{i(u_n)}^{ve}{}^{-1} : \boldsymbol{\sigma}_n + \mathbb{T}_{i,n+1}^{ve} \boldsymbol{C}_{i(u_{n+1})}^{ve}{}^{-1} : \boldsymbol{\sigma}_{n+1}^{(l)}\right] - \boldsymbol{\varepsilon}_{i,n+1}^{ve(l)} \tag{4.21}$$

$$\boldsymbol{R}_{j,n+1}^{\varepsilon^{ms,or(l+1)}} =$$

$$\left[\boldsymbol{\varepsilon}_{j,n}^{ms,or} \exp\left(\frac{-|\dot{u}|}{\tau_j} \right) + \mathbb{T}_{j,n}^{ms,or} \boldsymbol{C}_{j(u_n)}^{ms,or-1} : \boldsymbol{\sigma}_n + \mathbb{T}_{j,n+1}^{ms,or} \boldsymbol{C}_{j(u_{n+1})}^{ms,or \ -1} : \boldsymbol{\sigma}_{n+1}^{(l)} \right] - \boldsymbol{\varepsilon}_{j,n+1}^{ms,or(l)} \tag{4.22}$$

$$\boldsymbol{R}_{n+1}^{\varepsilon^{ms,tr(l+1)}} =$$

$$\left[\boldsymbol{\varepsilon}_{n}^{ms,tr} \exp\left(-\frac{-|\dot{U}|}{\tau_{tr}} \right) + \mathbb{T}_{n}^{ms,tr} \boldsymbol{C}_{(u_n)}^{ms,tr-1} : \boldsymbol{\sigma}_n + \mathbb{T}_{n+1}^{ms,tr} \boldsymbol{C}_{(u_{n+1})}^{ms,tr \ -1} : \boldsymbol{\sigma}_{n+1}^{(l)} \right] - \boldsymbol{\varepsilon}_{n+1}^{ms,tr(l)} \tag{4.23}$$

If $||\boldsymbol{R}_{n+1}^{\varepsilon(l+1)}|| \leq TOL3$, exit at the current iteration l. Otherwise, the stress increment for next iteration $(l+1)$ needs to be corrected as:

$$\boldsymbol{\sigma}_{n+1}^{(l+1)} = \boldsymbol{\sigma}_{n+1}^{(l)} + \delta_\Delta \boldsymbol{\sigma}_{n+1}^{(l+1)}$$

$$\delta_\Delta \boldsymbol{\sigma}_{n+1}^{(l+1)} = -\boldsymbol{C}_{n+1}^{T} : \left(\boldsymbol{R}_{n+1}^{\varepsilon^{el(l+1)}} + \sum_i \boldsymbol{R}_{i,n+1}^{\varepsilon^{ve(l+1)}} + \sum_j \boldsymbol{R}_{j,n+1}^{\varepsilon^{ms,or(l+1)}} + \boldsymbol{R}_{n+1}^{\varepsilon^{ms,tr(l+1)}} \right) \tag{4.24}$$

where the corresponding operator tensor can be derived from equations (3.2.5), (3.4.9), and (3.5.10-3.5.11):

$$\boldsymbol{C}_{n+1}^{T} = \left(\boldsymbol{C}_{n+1}^{ep(l) \ -1} + \sum_i \boldsymbol{C}_{i,n+1}^{ve \ -1} + \sum_j \boldsymbol{C}_{j,n+1}^{ms,or-1} + \boldsymbol{C}_{n+1}^{ms,tr-1} \right)^{-1} \tag{4.25}$$

$$\boldsymbol{C}_{i,n+1}^{ve \ -1} = \mathbb{T}_{i,n+1}^{ve} \boldsymbol{C}_{i(u_{n+1})}^{ve \ -1}, \ \boldsymbol{C}_{j,n+1}^{ms,or-1} = \mathbb{T}_{j,n+1}^{ms,or} \boldsymbol{C}_{j(u_{n+1})}^{ms,or \ -1}, \ \boldsymbol{C}_{n+1}^{ms,tr-1} = \mathbb{T}_{n+1}^{ms,tr} \boldsymbol{C}_{(u_{n+1})}^{ms,tr \ -1} \tag{4.26}$$

Consequently, the corresponding trial value for entering iteration $(l+1)$ becomes:

$$\Delta\boldsymbol{\varepsilon}_{i,n+1}^{ve,(l+1)} = \boldsymbol{R}_{i,n+1}^{\varepsilon^{ve(l+1)}} + \boldsymbol{\varepsilon}_{i,n+1}^{ve(l)} + \boldsymbol{C}_{i,n+1}^{ve \ -1} : \delta_\Delta \boldsymbol{\sigma}_{n+1}^{(l+1)} - \boldsymbol{\varepsilon}_{i,n}^{ve} \tag{4.27}$$

$$\Delta\boldsymbol{\varepsilon}_{j,n+1}^{ms,or(l+1)} = \boldsymbol{R}_{j,n+1}^{\varepsilon^{ms,or(l+1)}} + \boldsymbol{\varepsilon}_{j,n+1}^{ms,or(l)} + \boldsymbol{C}_{j,n+1}^{ms,or-1} : \delta_\Delta \boldsymbol{\sigma}_{n+1}^{(l+1)} - \boldsymbol{\varepsilon}_{j,n}^{ms,or} \tag{4.28}$$

$$\Delta\boldsymbol{\varepsilon}_{n+1}^{ms,tr(l+1)} = \boldsymbol{R}_{n+1}^{\varepsilon^{ms,tr(l+1)}} + \boldsymbol{\varepsilon}_{n+1}^{ms,tr(l)} + \boldsymbol{C}_{n+1}^{ms,tr-1} : \delta_\Delta \boldsymbol{\sigma}_{n+1}^{(l+1)} - \boldsymbol{\varepsilon}_{n}^{ms,tr} \tag{4.29}$$

Accordingly, following the elastic assumption, the trial stress for entering next m_LOOP becomes:

$$\Delta\boldsymbol{\sigma}_{n+1}^{(l+1,m=0)} = \boldsymbol{C}_{n+1}^{el \ -1} : \left(\Delta\boldsymbol{\varepsilon}_{n+1}^{\Delta\sigma} - \sum_i \Delta\boldsymbol{\varepsilon}_{n+1}^{ve,i(l+1)} - \sum_j \Delta\boldsymbol{\varepsilon}_{n+1}^{ms,j(l+1)} - \Delta\boldsymbol{\varepsilon}_{n+1}^{ms,tr(l+1)} \right) \tag{4.30}$$

5. Verification & validation

5.1. Verification

5.1.1. Test setup

Two benchmark testing cases are conducted on a quadratic brick element (C3D20) to verify the capability of the 3D rheological model. The test condition for Case 1 is set to be the same as in the work by Hassani et al. [32]. In Hassani et al. [32], a rheological model of wood has been provided, containing similar components as presented in this work. However, different constitutive laws are used, especially for the mechano-sorptive and plastic parts. A 40x40x40mm^3 cubic European beech (*Fagus sylvatica* L.) sample is subjected to a uniform compression load on the radial direction. Three confining symmetry planes are used, allowing free hydro-expansion. For simplification, Cartesian coordinate system is adopted. The test setup of this case is schematically shown in Fig. 5. Combinations of moisture flow and the mechanical load variations for both cases are shown in Fig. 6. Moisture transmission is assumed to be instantaneous. Hence, moisture content changes are
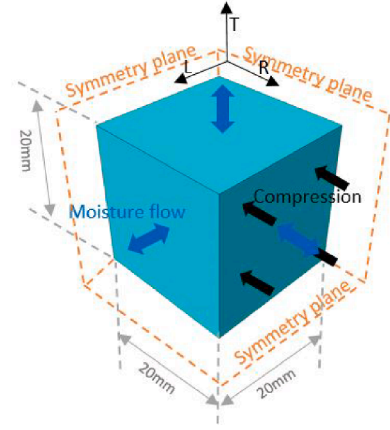

Fig. 5. Geometry and the finite element model.

applied directly as a pre-defined field in Abaqus.

In both cases, according to the change of mechanical loading and moisture content, seven stages are identified. Stage 1 (0 – 5 h), Stage 3 (55 – 60 h), Stage 5 (135 – 140 h) are the mechanical loading stages, where the mechanical load ramps to 10 MPa, 16 MPa, and 0 MPa for Case 1, and to 12 MPa, 16 MPa, and 0 MPa for Case 2.

In Stages 2, 4, and 7, mechanical load remains constant but moisture content starts to vary. Moisture content (u) remains constant for Case 1 during Stage 2 (5 – 55 h), but increases to 18% within 7.5 – 10 h for Case 2 and remains constant on 18% until Stage 4. During Stage 4 (60 – 135 h) and Stage 7 (200 – 290 h), the specimens in both cases are subjected to multiple moisture cycles between 18% and 12%. For Stage 6 (140 – 200 h), all conditions are kept constant.

5.1.2. Results of the verified model

Different strain components along the radial direction resulting from the loading conditions of the seven stages (presented in Fig. 6) are illustrated in Fig. 7. In order to observe the development of all partial strains in a clearer way, the hygro-expansion strain is subtracted from the total strain and the remaining shrinkage-corrected strain is presented in Fig. 7.

The results of the numerical analysis can be interpreted in the following way:

- Stage 1 (0 – 5 h): Linear elastic behaviour dominates for both cases.
- Stage 2 (5 – 55 h): In both cases, viscoelastic creep increases. In contrast to Case 1, during the moistening phase in Case 2, ordinary and transcending mechano-sorption strains are developed. Moreover, plastic strain can also be observed, which is due to the lowered yield strength caused by the moisture increase.
- Stage 3 (55 – 60 h): Both cases exhibit plastic deformation when the mechanical load increases. However, the magnitude of plastic deformation of Case 2 (u = 18%) is larger than Case 1(u = 12%), which can be explained by the moisture-dependent yield strength.
- Stage 4 (60 – 135 h): Both viscoelastic creep and the ordinary mechano-sorption increase in the two cases. Both moistening and de-moistening lead to the increase of mechano-sorptive deformation. However, at the first moisture increase cycle at this stage in Case 1, both plastic deformation and transcending mechano-sorption are increased. Moreover, the magnitude of plastic deformation in Case 1 reaches the same level as achieved in Case 2 from the previous stages. The magnitude of transcending mechano-sorption is greater in Case 1 compared to Case 2.
- Stage 5 (135 – 140 h): During unloading, the instantaneous elastic response is immediately compensated for both cases.
- Stage 6 (140 – 200 h): Viscoelastic creep is partly recovered for both cases.
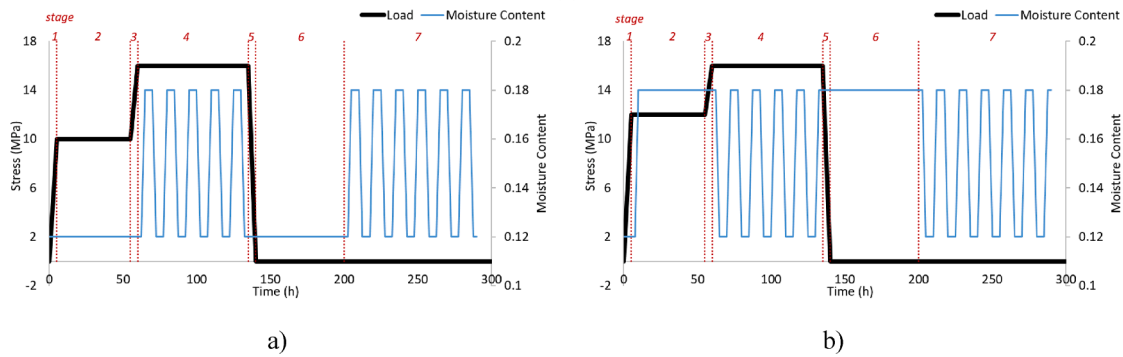- Stage 7 (200 – 290 h): For both cases, the ordinary mechano-

Fig. 6. Mechanical loading and moisture variation conditions for a) Case 1; b) Case 2.Vertical red lines represent the boundaries of different stages. (For interpretation of the references to colour in this figure legend, the reader is referred to the web version of this article.)
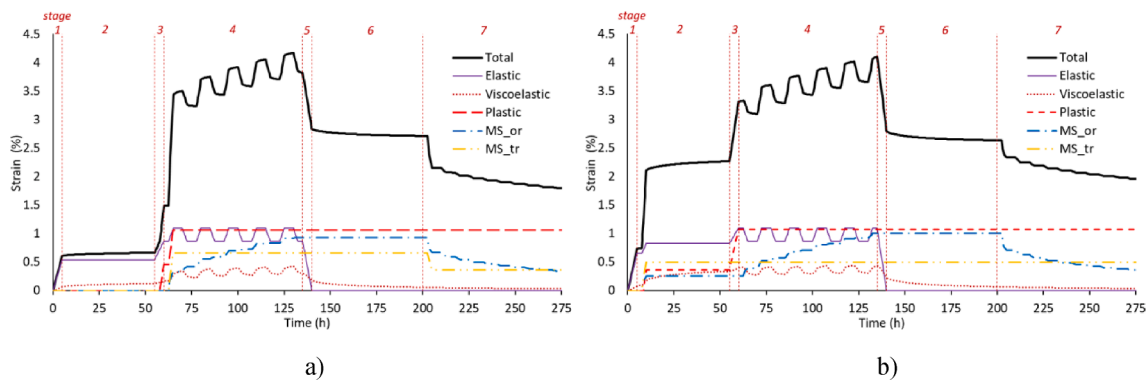

Fig. 7. Evolution of the total strain and its different components in radial direction for a) Case 1; b) Case 2.

sorption strain decreases continuously during the moistening and de-moistening periods. No recovery of transcending mechano-sorption change is observed in Case 2, while a considerable extent of recovery transcending mechano-sorption strain is observed in Case 1.

5.1.3. Discussions on the verified model

The different loading conditions in the two cases provide a clear illustration of the behaviour of each model components. The evolution of elastic deformation and viscoelastic creep is dominated by the mechanical load, while the moisture cycles result in fluctuations, which is due to the moisture-dependent elastic and viscoelastic stiffnesses. Plastic deformation occurs at the time when the mechanical load increases (Stage 3 in both cases) and when the first moistening under a stress level starts (Stage 4 in Case 1 and Stage 2 in Case 2), since the yielding strength decreases when moisture content increases. Both transcending and ordinary mechano-sorptions are driven by moisture variation, hence they stay constant when moisture content remains constant (Stage 6 in both cases and Stage 2 in Case 1).

The ordinary mechano-sorptive strain continues to creep at Stage 4 in both cases, but the creep rate decreases, since the Kelvin-Voigt elements are gradually reaching the creep limit. Although only partial recovery is observed in the ordinary mechano-sorptive part in the current test period, it is anticipated to recover until full-extent according to the full-recoverable nature of Kelvin-Voigt elements. In contrast, the transcending mechano-sorptive recovery occurs only when moisture content is surpassing the critical value at the start of the current load level (i.e. when transcending moisture content U increases). This explains the different recovery behaviors at Stage 7 in both cases. Moreover, as the recovery rate is slower than the creep rate for Kelvin-Voigt element, the transcending mechano-sorptive recovery appears to be only partial, even when experiencing the same ΔU in the recovery and loading phases.

The test setup for Case 1 is set to be identical to the test example 1, presented in the study of Hassani et al. [32]. As a result, it can be seen that apart from the additional transcending mechano-sorptive component, the rest of the components (elastic, viscoelastic, ordinary mechano-sorption, and plastic) evolve in the same pattern and of the same order of magnitude. The difference between these both models can indicate that Hassani's model may underestimate the mechano-sorptive creep and recovery, at the first moisture increase in loading and recovery phase, respectively. Moreover, the hardening parameters determined according to different works [32,72] showed possible discrepancies (Table A5). To keep the resultant plastic strain in the same order of magnitude as calculated by Hassani's model and to provide a better comparison between the two models, values calibrated based on the study of Hassani et al. [32] are adopted here. Nevertheless, it must be mentioned that no experimental validation is conducted for this test setup in both works.

5.2. Validation 1

5.2.1. Test setup

In order to validate the current model, simulation results are compared to the experimental results of two creep-recovery tests realized by Randriambololona [21] on small clear specimens of maritime pine (*Pinus Pinaster*). Information about the FEM model is given in Fig. 8. The specimen is subjected to a tensile load of 16 MPa and 32 MPa in the longitudinal direction in Case 1 and Case 2, respectively. Relative humidity is cycling between 30% and 75% during both loading and unloading phases, as shown in Fig. 9.

Specimens with the dimension of 30x3x0.7 mm³ are taken from different locations of the same tree. Due to the small dimensions of the samples, Cartesian coordinate system is used for simplification. Three symmetry planes are defined and the moisture flow is allowed in the two

transverse directions. Although samples are taken from the same tree, the mechanical properties of the specimen may vary strongly. According to Randriambololona [21], specimens in Case 2 exhibit higher elastic stiffness and lower hydro-expansion coefficient in longitudinal direction compared to the specimens in Case 1. Viscoelastic and mechano-sorptive parameters are calibrated according to the experimental results using the least-square approach. Plasticity is not considered in this set of analysis as the load level is below the yield strength [73].

5.2.2. Results and discussions

Besides validating the model in this case, sensitivity analysis is performed here by calibrating the parameters that are contributing to the viscoelasticity or mechano-sorptive behaviours to check the possibility for model generalization and implementation to different setups. Fig. 10 shows three sets of simulation results in comparison to the experimental results and the contribution of each viscoelastic and mechano-sorptive components. The differences stem from the ways how the viscoelastic and mechano-sorptive parameters are calibrated:

- Calibration 1: parameters are calibrated using least-square approach based on the experimental results in Case 1 (Fig. 10a) and applied to Case 2 (Fig. 10b);
- Calibration 2: parameters are calibrated using least-square approach based on the experimental results in Case 2 (Fig. 10d) and applied to Case 1 (Fig. 10c);
- Calibration 3: parameters are calibrated using least-square approach based on the experimental results in both Case 1 (Fig. 10e) and Case 2 (Fig. 10f).

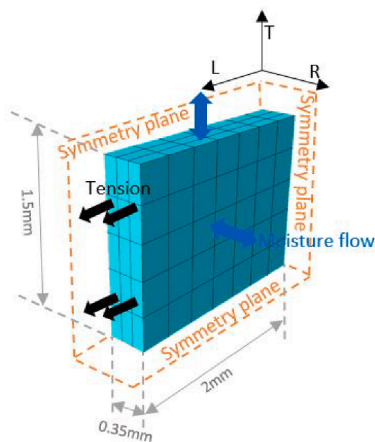In Calibration 1 and 2, it can be seen that agreements of Fig. 10a and

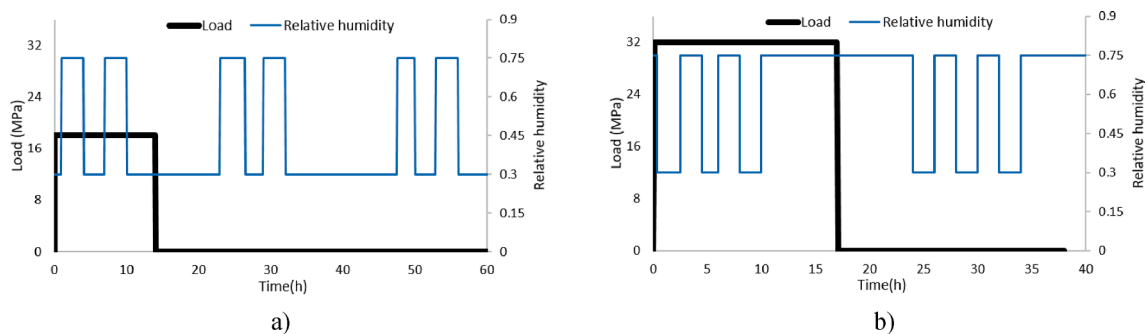Fig. 10d are better than the ones in Calibration 3. Yet, when applied to the other case, the simulation results deviate from the experimental values. However, in Calibration 1, applying the calibrated parameters to Case 2 (Fig. 10b), the general behaviour still correspond to the experiment, despite the higher creep rates. In Calibration 2, since the transcending mechano-sorptive part has a significant contribution to the strain evolution in Case 1 but no influence in Case 2, the stiffness tensor of transcending mechano-sorptive part remains zero when calibrated based on the information from Case 2. As a result, large discrepancy is observed in Fig. 10c due to the missing of transcending mechano-sorptive parameters.

Considering the agreement for both cases, Calibration 3 showed the best performance. As a result, two Kelvin-Voigt elements for viscoelastic part and two for the ordinary mechano-sorptive part are adopted. The small number of elements required is due to the very short period of experiment, as no information of the longer periods is provided for calibration. Hence, it is anticipated that there would be some discrepancy between the simulation and experimental results when the current model is applied to long-term tests.

5.3. Validation 2

5.3.1. Test setup

The reference experimental data used for this set of validation was obtained from the studies of Toratti and Svensson [19,74]. Here, clear heartwood samples of Scots pine (*Pinus sylvestris*) with cross section of 10×20 mm^2 were used. The measurement point is 18 mm away from the symmetry plane, as shown in Fig. 11. Before testing, the specimens were conditioned at room temperature (T = 20 °C) and relative humidity RH = 60% for 1 year. Two cases of test conditions are selected for this work (Fig. 12). Both the loading and the measuring direction coincide with the tangential direction of the wood for all the studied specimens. For the numerical simulation, 168 quadratic elements C3D20T are used as shown in Fig. 11. Combinations of moisture flow and the mechanical load variations for both cases are shown in Fig. 12.

Fortino et al. [28] proposed a 3D rheological model based on the one-dimensional model developed in the study of Svensson and Toratti [19]. The model showed a good agreement with the medium-term experimental results, yet it could not correctly capture the recovery that can be observed in the short-term experiments [74]. In this work, simulation results calculated by the current generalized model (referred as Model 2) and a model constructed according to Fortino et al. [28] (referred as Model 1) are both compared with the experimental results. Both models are based on the 1D model proposed in the study of Svensson and Toratti [19]. However, one major difference lies in the transcending mechano-sorptive part, which is the comparable to the irrecoverable mechano-sorptive part ($\varepsilon^{ms,irr}$) in the study of Fortino et al. [28]. The ordinary mechano-sorptive part is the same as the recoverable mechano-sorptive part in the study of Fortino et al. [28], using three Kelvin-Voigt elements
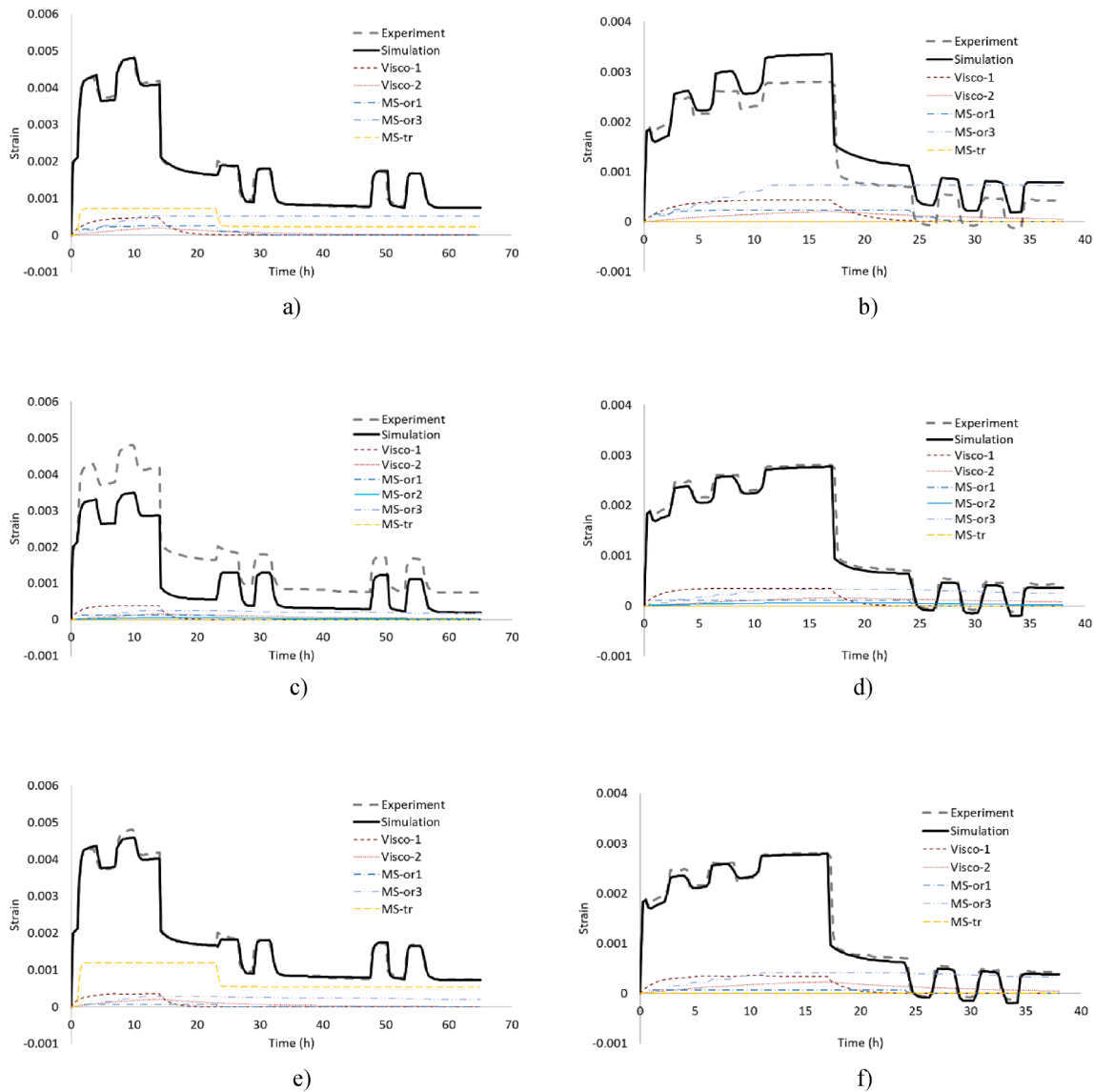

Fig. 8. Geometry and the finite element model.

Fig. 9. Mechanical loading and moisture variation conditions for a) Case 1; b) Case 2.

Fig. 10. Evolution of the total strain and its different components in longitudinal direction for a,c,e) Case 1; b,d,f) Case 2.
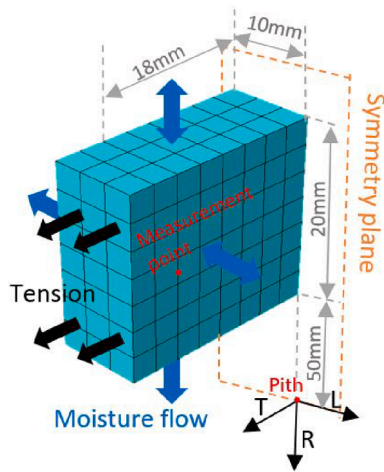

Fig. 11. Geometry and the finite element model.

in series, as can be seen in the following equation (5.1) and equations (3.5.6-3.5.7):

$$
\begin{cases}
\dot{\varepsilon}_j^{ms,r} = \dfrac{C_j^{ms,r\,-1} : \sigma - \varepsilon_i^{ms,r}}{\tau_j} |\dot{u}| \\[2ex]
\dot{\varepsilon}^{ms,irr} = C^{ms,irr\,-1} : \sigma |\dot{U}|
\end{cases}
\tag{5.1}
$$

5.3.2. Results

Fig. 13 shows the resultant shrinkage-corrected strains of the original model (Model 1) and the modified model (Model 2) in comparison to the short- and medium-term experimental results (free-shrinkage strain). It can be seen that Model 2 captures the recovery during moisture change after unloading in the short-term experiment and retains a good agreement with the medium-term experiment.

5.3.3. Discussions

To better visualize the contribution of different parts of the mechano-sorption, Fig. 14 shows the decomposed strain of the three recoverable Kelvin elements and the irrecoverable dashpot. In the short-term test, during the first adsorption, the strain of the irrecoverable dashpot is almost double the sum of the three Kelvin elements. However, in the
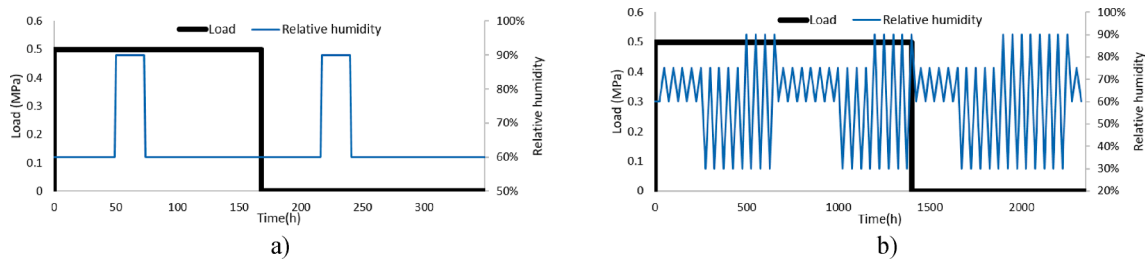
Fig. 12. Mechanical loading and moisture variation conditions for a) Case 1 (short-term); b) Case 2 (medium- term).
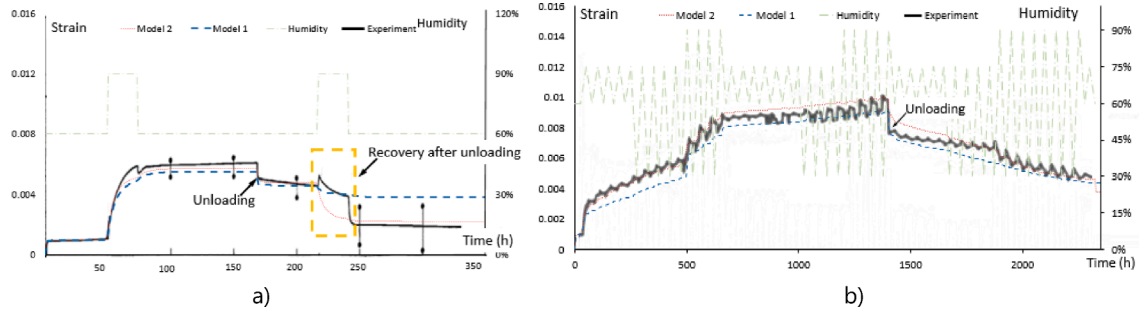

Fig. 13. Evolution of the total strain and its different components in tangential direction for a) Case 1; b) Case 2.
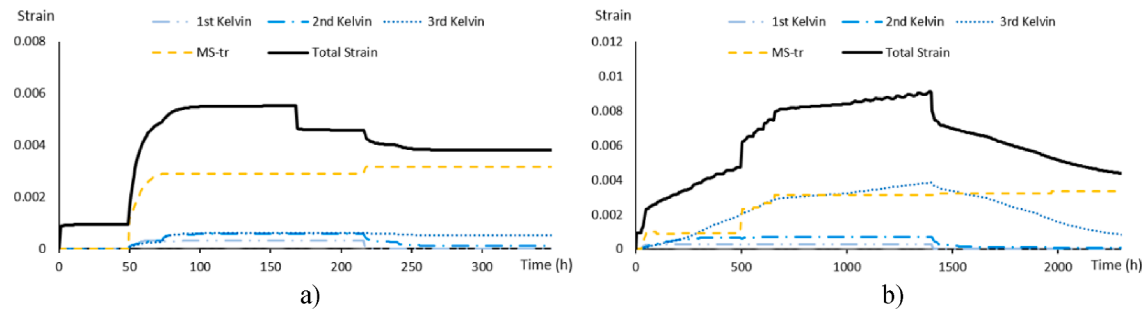

Fig. 14. Decomposition of mechano-sorptive strain into each element for Model 1: a) short-; b) medium-term test.
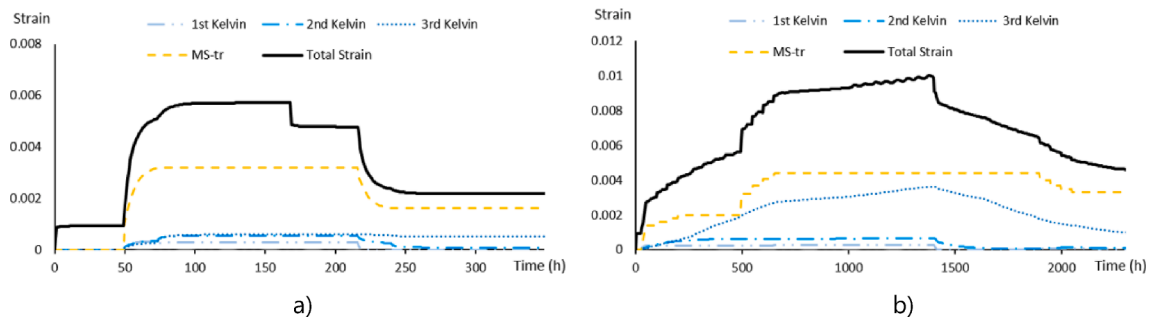

Fig. 15. Decomposition of mechano-sorptive strain into each element for Model 2: a) short- b) medium-term test.

desorption phase under loading, no increase is exhibited in the dashpot, since the U does not get updated. After unloading, the 1st and the 2nd Kelvin elements exhibit recovery. Due to the large retardation time of the 3rd Kelvin element ($\tau_3 = 1$), its recovery is minor. On the contrary, in the medium-term test, the contribution of the 3rd Kelvin element is significant in both creep and recovery phases. However, the strains of the 1st and 2nd Kelvin elements remain small, as both elements reach their creep limits after a few cycles, i.e. the dashpot is "empty" and the stress-strain ratio equals to the stiffness of the spring in the Kelvin element.

Fig. 15 shows the contribution of different mechano-sorption parts of Model 2. In comparison to the results shown in Fig. 14, the main difference comes from the transcending part of Model 2 and the

irrecoverable part of Model 1. In the simulation for the short-term test, since the specimen is subjected to an increase in moisture content that exceeds the initial value at the unloading point, a large recovery is exhibited in the newly modified part (the MS-tr component in Fig. 15), which is the main source of the total recovery. In the simulation for the medium-term test, as the specimen is unloaded at a high moisture content point, the U value hardly gets updated during the unloading phase, hence the total behaviour is kept similar to Model 1, also retaining a good agreement with the experimental results. As a conclusion, based on the current simulation results, Model 2 successfully introduces the recovery feature while retaining almost fully the capability of the initial Model 1.

6. Conclusions

In this paper, a 3D orthotropic elastic-plastic viscoelastic mechano-sorptive model for wood is generalized. The constitutive model is based on the 3D model developed by Fortino et al. [28], with addition of plasticity and modification in mechano-sorption. The modified mechano-sorptive component in this study is composed of the ordinary and transcending parts, addressing the complex mechano-sorptive characteristics, which are dependent on the moisture history. Kelvin-Voigt elements are used for the viscoelastic and mechano-sorptive mechanisms, and Hill's [63] criterion with isotropic hardening is used to describe the elastic–plastic mechanism. These elements are integrated in a serial form with the elasticand hydro-expansion strain. Parameters that are contributing to the elastic, viscoelastic and mechano-sorptive components are moisture dependent. The constitutive model and the algorithm for stress update are implemented into a UMAT subroutine of the FEM framework Abaqus. A semi-coupled moisture-stress analysis is performed. Verification and validation of the model based on the previously performed studies showed that the model is capable of describing wood behavior under varying combinations of mechanical load and humidity changes. The transcending mechano-sorptive creep and the complicated mechano-sorptive recovery is well captured. Sensitivity analysis is also performed and the model is capable of capturing the general mechanical behavior for different wood species and for different combinations of mechanical load and moisture variation. In addition, it needs to be mentioned that the different influence of tensile and compressionstress on the mechano-sorptive creep rate is not taken into account. The capability of this model when extrapolated to longer load durations needs to be validated by more experimental data. For further development, the model can be associated with damage/failure mechanisms to evaluate the material capacity under varying environments.

CRediT authorship contribution statement

Taoyi Yu: Methodology, Software, Writing – original draft, Writing – review & editing. **Ani Khaloian:** Conceptualization, Methodology, Writing – review & editing, Supervision, Project administration, Funding acquisition. **Jan-Willem van de Kuilen:** Conceptualization, Writing – review & editing, Supervision, Project administration, Funding acquisition.

Declaration of Competing Interest

The authors declare that they have no known competing financial interests or personal relationships that could have appeared to influence the work reported in this paper.

Acknowledgement

Appendix

The parameters of different species are listed in the following tables. The parameters without mentioning the references are calibrated in this work.

Table A1
Elastic parameters.

	E_R [MPa]	E_T [MPa]	E_L [MPa]	G_{RT} [MPa]	G_{RL} [MPa]	G_{TL} [MPa]	v_{LT}	v_{TR}	v_{LR}	u_{ref}	b_i [MPa]
European Beech [32]	1845	591	14,255	486	1385	922	0.228	0.281	0.278	12%	−3.5
Scot Pine [28]	900	500	12,000	40	700	700	0.360	0.310	0.510	12%	2.6
Maritime Pine(Case1)	731	452	9500	62	633	559	0.430	0.310	0.390	12%	2.6
Maritime Pine(Case2)	1411	873	18,341	120	1223	1079	0.430	0.310	0.390	12%	2.6

* for Maritime Pine, the longitudinal modulus is provided in [21], the ratio between other parameters with longitudinal modulus is taken from [75].
* a uniform b_i value is selected for all the engineering constants as a simplification [28].

Table A2
Hydro-expansion coefficients.

	α_R^u	α_T^u	α_L^u	β_L^u
European Beech [32]	0.191	0.462	0.011	1.8
Scot Pine [28]	0.17	0.33	0.005	1.8
Maritime Pine (Case 1)	0.175	0.307	0.027	0.5
Maritime Pine (Case 2)	0.175	0.307	0.017	0.5

* for Maritime Pine, the longitudinal coefficient is provided in [21] and transverse coefficients are taken from [76].
* only transverse components of β^u are assumed to be 0 as a simplification.

Table A3
Viscoelastic parameters.

	τ_1 [s]	J_1^{ve} [1/MPa]	τ_2 [s]	J_2^{ve} [1/MPa]	τ_3 [s]	J_3^{ve} [1/MPa]	τ_4 [s]	J_4^{ve} [1/MPa]	u_{ref}	β_i^{ve} [1/MPa]
European Beech [32]	2132	0.150	219,096	0.123	32,040	0.088	12,339,540	0.679	15%	1.2
Scot Pine [28]	8640	0.085	86,400	0.035	864,000	0.070	8,640,000	0.200	–	–
Maritime Pine	6036	0.192	48,564	0.179	–	–	–	–	–	–

* a uniform β_i^{ve} value is selected for all the Kelvin component as a simplification.

Table A4

Mechano-sorptive parameters.

	τ_1	$J_{1,T}^{ms}$ [1/MPa]	$J_{1,L}^{ms}$ [1/MPa]	τ_2	$J_{2,T}^{ms}$ [1/MPa]	$J_{2,L}^{ms}$ [1/MPa]	τ_3	$J_{3,T}^{ms}$ [1/MPa]	$J_{3,L}^{ms}$ [1/MPa]	τ_{tr}	$J^{ms,tr}$ [1/MPa]
European Beech [32]	0.01	0.0004	0.1142	0.1	0.0004	0.320	1	0.003	0.023	0.1	0.011
Scot Pine	0.01	0.0006	0.175	0.1	0.0015	0.490	1	0.009	0.035	0.1	0.016
Maritime Pine	0.01	0.0001	0.037	–	–	–	1	0.302	1.174	0.044	1.215

Table A5

Plastic parameters for European beech [32,72]

	$f_{R(u)}$	$f_{T(u)}$	$f_{L(u)}$	$f_{RT(u)}$	$f_{RL(u)}$	$f_{TL(u)}$
$f_{i,ref}$ [MPa]	11.637	4.839	51.34	3.164	9.684	10.419
β_i^f [MPa]	−57.89	−20.84	−350.4	−12.13	−38.84	−38.61

* the moisture dependent strength value is calculated as $f_{i(u)} = f_{i,ref} + \beta_i^f * (u - u_{ref})$ with $u_{ref} = 15\%$.

* the hardening parameter b and Q determined according to [32] are 0.4 and 120 MPa, and according to test results in [72] are 5 and 120 MPa.

References

[1] Armstrong LD, Christensen GN. Influence of moisture changes on deformation of wood under stress. Nature 1961;191(4791):869–70. https://doi.org/10.1038/191869a0.

[2] Hearmon RF. Moisture content changes and creep of wood. Forest Prod J 1964;14: 357–9.

[3] Winter S, Kreuzinger H. The Bad Reichenhall ice-arena collapse and the necessary consequences for wide span timber structures. WCTE; 2008.

[4] Frühwald E, Serrano E, Toratti T, Arne E, Sven T. Design of safe timber structures. How can we learn from structural failures in concrete, steel and timber? [Report TVBK-3053].Lund, Sweden, 2008.

[5] Van de Kuilen JWG. Service life modelling of timber structures. Mater Struct 2007; 40(1):151–61. https://doi.org/10.1617/s11527-006-9158-0.

[6] European Committee for Standardisation. EN 1995-1-1: Eurocode 5: Design of timber structures - Part 1-1: General - Common rules and rules for buildings.

[7] Mark RE. Mechanical behavior of the molecular components of fibers. In: Jayne B A, editor. Theory and design of wood and fiber composite materials. Syracuse Univ. Pr. S.l; 1972.

[8] Gibson EJ. Creep of wood: role of water and effect of a changing moisture content. Nature 1965;206(4980):213–5. https://doi.org/10.1038/206213a0.

[9] Van der Put TACM. Deformation and damage processes in wood [Doctoral dissertation].Delft. Delft: University Press; 1989.

[10] Boyd JD. An anatomical explanation for visco-elastic and mechano-sorptive creep in wood, and effects of loading rate on strength. In: Baas P, editor. New Perspectives in Wood Anatomy. Netherlands, Dordrecht: Springer; 1982.

[11] Hoffmeyer P, Davidson RW. Mechano-sorptive creep mechanism of wood in compression and bending. Wood Sci. Technol. 1989;23(3):215–27. https://doi.org/10.1007/BF00367735.

[12] Hanhijrvi A. Deformation kinetics based rheological model for the time-dependent and moisture induced deformation of wood. Wood Sci Technol 1995;29:191–9. https://doi.org/10.1007/BF00204585.

[13] Schänzlin J. Modeling the long-term behavior of structural timber for typical serviceclass-II-conditions in South-West Germany [Habilitation].Stuttgart. Universität Stuttgart 2010.

[14] Mukudai J, Yata S. Further modeling and simulation of viscoelastic behavior (bending deflection) of wood under moisture change. Wood Sci Technol 1987;21: 49–63. https://doi.org/10.1007/BF00349717.

[15] Alfthan J. The effect of humidity cycle amplitude on accelerated tensile creep of paper. Mech Time-Depend Mater 2004;8(4):289–302. https://doi.org/10.1007/s11043-004-0536-0.

[16] Leicester RH. A rheological model for mechano-sorptive deflections of beams. Wood Sci Technol 1971;5(3):211–20. https://doi.org/10.1007/BF00353683.

[17] Ranta-Maunus A. The viscoelasticity of wood at varying moisture content. Wood Sci Technol 1975;9(3):189–205. https://doi.org/10.1007/BF00364637.

[18] Hanhijärvi A. Advances in the knowledge of the influence of moisture changes on the long-term mechanical performance of timber structures. Mat Struct 2000;33 (1):43–9. https://doi.org/10.1007/BF02481695.

[19] Svensson S, Toratti T. Mechanical response of wood perpendicular to grain when subjected to changes of humidity. Wood Sci Technol 2002;36(2):145–56. https://doi.org/10.1007/s00226-001-0130-4.

[20] Mårtensson A. Mechano-sorptive effects in wooden material. Wood Sci Technol 1994;28:437–49. https://doi.org/10.1007/BF00225463.

[21] Randriambololona H. Modélisation du comportement différé du bois en environnement variable [Doctorate dissertation].France. University of Limoges; 2003.

[22] Toratti T. Creep of timber beams in a variable environment [Doctorate dissertation].Helsinki. Espoo: University of Technology; 1992.

[23] Zhou HZ, Zhu EC, Fortino S, Toratti T. Modelling the hygrothermal stress in curved glulam beams. J Strain Anal Eng Design 2010;45(2):129–40. https://doi.org/10.1243/03093247JSA563.

[24] Fortino S, Hradil P, Genoese A, Genoese A, Pousette A. Numerical hygro-thermal analysis of coated wooden bridge members exposed to Northern European climates. Constr Build Mater 2019;208:492–505. https://doi.org/10.1016/j.conbuildmat.2019.03.012.

[25] Massaro FM, Malo KA. Modelling the viscoelastic mechanosorptive behaviour of Norway spruce under long-term compression perpendicular to the grain. Holzforschung 2019;73:715–25. https://doi.org/10.1515/hf-2018-0218.

[26] O'Ceallaigh C, Sikora K, McPolin D, Harte AM. Modelling the hygro-mechanical creep behaviour of FRP reinforced timber elements. Constr Build Mater 2020;259: 119899. https://doi.org/10.1016/j.conbuildmat.2020.119899.

[27] Santaoja K. Mechano-sorptive structural analysis of wood by the ABAQUS finite element program [Research Notes].Valtion teknillinen tutkimuskeskus, Tiedotteita - Statens tekniska forskningscentral, Meddelanden. Espoo, Helsinki: Technical Reserch Centre of Finland; 1991.

[28] Fortino S, Mirianon F, Toratti T. A 3D moisture-stress FEM analysis for time dependent problems in timber structures. Mech Time-Depend Mater 2009;13(4): 333–56. https://doi.org/10.1007/s11043-009-9103-z.

[29] Vidal-Sallé E, Chassagne P. Constitutive equations for orthotropic nonlinear viscoelastic behaviour using a generalized maxwell model application to wood material. Mech Time-Depend Mater 2007;11(2):127–42. https://doi.org/10.1007/s11043-007-9037-2.

[30] Hanhijärvi A, Mackenzie-Helnwein P. Computational analysis of quality reduction during drying of lumber due to irrecoverable deformation. I: orthotropic viscoelastic-mechanosorptive-plastic material model for the transverse plane of wood. J Eng Mech 2003;129(9):996–1005. https://doi.org/10.1061/(ASCE)0733-9399(2003)129:9(996).

[31] Husson JM, Dubois F, Sauvat N. Elastic response in wood under moisture content variations: analytic development. Mech Time-Depend Mater 2010;14(2):203–17. https://doi.org/10.1007/s11043-009-9104-y.

[32] Hassani MM, Wittel FK, Hering S, Herrmann HJ. Rheological model for wood. Comput Methods Appl Mech Eng 2015;283:1032–60. https://doi.org/10.1016/j.cma.2014.10.031.

[33] Qiu L. Performance of Curved Glulam Beams Under Load and Moisture Variations [Doctoral dissertation].Harbin Institute of Technology. China: Harbin; 2015.

[34] Martensson A, Thelandersson S. Effect of moisture and mechanical loading on wooden materials. Wood Sci Technol 1990;24(3):247–61. https://doi.org/10.1007/BF01153558.

[35] Hunt DG, Shelton CF. Longitudinal moisture-shrinkage coefficients of softwood at the mechano-sorptive creep limit. Wood Sci Technol 1988;22(3):199–210. https://doi.org/10.1007/BF00386014.

[36] Mårtensson A. Mechanical Behaviour of Wood Exposed to Humidity Variations [Doctoral dissertation].Lund. University; 1992.

[37] Sandhaas C. Mechanical behviour of timber joints with slotted-in steel plates [Doctoral dissertation]. Wöhrmann Zutphen, 2012. ISBN: 9789085708377.

[38] Hunt DG. Linearity and non-linearity in mechano-sorptive creep of softwood in compression and bending. Wood Sci Technol 1989;23(4):323–33. https://doi.org/10.1007/BF00353248.

[39] Salin J-G. Numerical prediction of checking during timber drying and a new mechano-sorptive creep modelQuantitatives Vorhersagen der Rißbildung bei der Holztrocknung und ein neues Modell des mechanisch-sorptiven Kriechens. Holz als Roh-und Werkstoff 1992;50(5):195–200. https://doi.org/10.1007/BF02663286.

[40] Yahiaoui K. A rheological model to account for mechano-sorptive behavior. In: COST 508 Work Shop on "'Fundamental aspects on creep in wood", 1991, Lund Sweden.

[41] Becker P. Modellierung des zeit-und feuchteabhängigen Materialverhaltens zur Untersuchung des Langzeittragverhaltens von Druckstäben aus Holz [Doctoral dissertation].Bauhaus. Weimar: Universität; 2002.

[42] Mårtensson A, Svensson S. Stress-strain relationship of drying wood. part 2: verification of a one-dimensional model and development of a two-dimensional model. Holzforschung 1997;51(6):565–70. https://doi.org/10.1515/hfsg.1997.51.6.565.

[43] Svensson S, Mårtensson A. Simulation of drying stresses in wood. Holz als Roh- und Werkstoff 2002;60(1):72–80. https://doi.org/10.1007/s00107-001-0266-9.

[44] Huč S, Svensson S, Hozjan T. Hygro-mechanical analysis of wood subjected to constant mechanical load and varying relative humidity. Holzforschung 2018;72: 863–70. https://doi.org/10.1515/hf-2018-0035.

[45] Hanhijärvi A. Deformation properties of Finnish spruce and pine wood in tangential and radial directions in association to high temperature drying. part IV. verformungseigenschaften von finnischem Fichten- und Kiefernholz in tangentialer und radialer Richtung unter Bedingungen der Hochtemperaturtrocknung. Teil IV. Model Holz als Roh- und Werkstoff 2000;58(4):211–6. https://doi.org/10.1007/s001070050415.

[46] Hunt DG, Gril J. Evidence of a physical ageing phenomenon in wood. J Mater Sci Lett 1996;15(1):80–2. https://doi.org/10.1007/BF01855620.

[47] Bažant ZP. Constitutive equation of wood at variable humidity and temperature. Wood Sci Technol 1985;19(2):159–77. https://doi.org/10.1007/BF00353077.

[48] Bou Saïd E. Contribution à la modélisation des effets différés du bois et du béton sous conditions climatiques variables. Application aux structures mixtes bois-béton. [Doctoral Dissertation].Ingénieur Structures Génie Civil de l'Université Libanaise, 2003.

[49] Chassagne P, Saïd EB, Jullien JF, Galimard P. Three dimensional creep model for wood under variable humidity-numerical analyses at different material scales. Mech Time-Depend Mater 2005;9(4):1–21. https://doi.org/10.1007/s11043-005-9001-y.

[50] Mukudai J, Yata S. Modeling and simulation of viscoelastic behavior (tensile strain) of wood under moisture change. Wood Sci Technol 1986;20(4):335–48. https://doi.org/10.1007/BF00351586.

[51] Mukudai J, Yata S. Verification of Mukudai's mechano-sorptive model. Wood Sci Technol 1988;22(1):43–58. https://doi.org/10.1007/BF00353227.

[52] Gril, J. Modelling mechano-sorption in wood through hygro-locks and other approaches. International Symposium on Wood Science and Technology (IAWPS 2015) and 60th. Anniversary of the Japan Wood. Research Society.

[53] Gril J. Une modélisation du comportement hygro-rhéologique du bois à partir de sa microstructure [Doctoral dissertation].Université. Paris 1988;6.

[54] Colmars J, Dubois F, Gril J. One-dimensional discrete formulation of a hygrolock model for wood hygromechanics. Mech Time-Depend Mater 2014;18(1):309–28. https://doi.org/10.1007/s11043-013-9229-x.

[55] Dubois F, Randriambololona H, Petit C. Creep in wood under variable climate conditions: numerical modeling and experimental validation. Mech Time-Depend Mater 2005;9(2-3):173–202. https://doi.org/10.1007/s11043-005-1083-z.

[56] Dubois F, Husson J-M, Sauvat N, Manfoumbi N. Modeling of the viscoelastic mechano-sorptive behavior in wood. Mech Time-Depend Mater 2012;16(4): 439–60. https://doi.org/10.1007/s11043-012-9171-3.

[57] Saifouni O. Modélisation des effets rhéologiques dans les matériaux : application au comportement mécanosorptif du bois [Doctoral thesis].Université Blaise Pascal -. Clermont-Ferrand II, France 2014.

[58] Nguyen SL, Destrebecq JF. An orthotropic incremental model for the hydromechanical behaviour of. softwood 2015. https://doi.org/10.26168/ICBBM2015.59.

[59] Navi P, Stanzl-Tschegg S. Micromechanics of creep and relaxation of wood. a review COST Action E35 2004–2008: Wood machining – micromechanics and fracture. Holzforschung 2009;63. https://doi.org/10.1515/HF.2009.013.

[60] Grossman PUA. Requirements for a model that exhibits mechano-sorptive behaviour. Wood Sci Technol 1976;10(3):163–8. https://doi.org/10.1007/BF00355737.

[61] Hanhijärvi A. Modelling of creep deformation mechanisms in wood [Doctoral dissertation]. VTT Technical Research Centre of Finland. Espoo 1995.

[62] Toratti T. Modelling the creep of timber beams. Rakenteiden Mekaniikka 1992;25: 12–35.

[63] Hill R. A theory of the yielding and plastic flow of anisotropic metals. Proc R Soc Lond A 1948;193:281–97. https://doi.org/10.1098/rspa.1948.0045.

[64] Kharouf N, McClure G, Smith I. Elasto-plastic modeling of wood bolted connections. Comput Struct 2003;81(8-11):747–54. https://doi.org/10.1016/S0045-7949(02)00482-0.

[65] Zhang L, Xie Q, Zhang B, Wang L, Yao J. Three-dimensional elastic-plastic damage constitutive model of wood. Holzforschung 2021;75:526–44. https://doi.org/10.1515/hf-2019-0247.

[66] Mackenzie-Helnwein P, Eberhardsteiner J, Mang HA. A multi-surface plasticity model for clear wood and its application to the finite element analysis of structural details. Comput Mech 2003;31(1-2):204–18. https://doi.org/10.1007/s00466-003-0423-6.

[67] Guan ZW, Zhu EC. Finite element modelling of anisotropic elasto-plastic timber composite beams with openings. Eng Struct 2009;31(2):394–403. https://doi.org/10.1016/j.engstruct.2008.09.007.

[68] Wang M, Song X, Gu X. Three-dimensional combined elastic-plastic and damage model for nonlinear analysis of wood. J Struct Eng 2018;144(8):04018103. https://doi.org/10.1061/(ASCE)ST.1943-541X.0002098.

[69] Rosen HN. The influence of external resistance on moisture adsorption rates in wood. Wood Fiber Sci 1978;10:218–28.

[70] Avramidis S, Siau J. An investigation of the external and internal resistance to moisture diffusion in wood. Wood Sci Technol 1987;21:249–56. https://doi.org/10.1007/BF00351396.

[71] Simo JC, Hughes TJR. Computational inelasticity. Cham: Springer International Publishing; 1998.

[72] Hering S, Niemz P. Moisture-dependent, viscoelastic creep of European beech wood in longitudinal direction. viskoelastisches Kriechverhalten von Rotbuche in longitudinaler Richtung bei verschiedenen Holzfeuchten. Eur J Wood Prod 2012; 70(5):667–70. https://doi.org/10.1007/s00107-012-0600-4.

[73] Dias AMPG, Van de Kuilen JWG, Cruz HMP, Lopes SMR. Numerical Modeling of the Load-Deformation Behavior of Doweled Softwood and Hardwood Joints. WFS 2010:480–9.

[74] Toratti T, Svensson S. Mechano-sorptive experiments perpendicular to grain under tensile and compressive loads. Wood Sci Technol 2000;34(4):317–26. https://doi.org/10.1007/s002260000059.

[75] Aira JR, Arriaga F, Íñiguez-González G. Determination of the elastic constants of Scots pine (Pinus sylvestris L.) wood by means of compression tests. Biosyst Eng 2014;126:12–22. https://doi.org/10.1016/j.biosystemseng.2014.07.008.

[76] Cruz H, Jones D, Nunes L. Wood. In: Gonçalves MC, Margarido F, editors. Materials for Construction and Civil Engineering. Cham: Springer International Publishing; 2015. p. 557–83. https://doi.org/10.1007/978-3-319-08236-3_12.

[77] Ormarsson S. Numerical analysis of moisture-related distortions in sawn timber [Doctoral dissertation]. Sweden: Chalmers University of Technology; 1999.

[78] Caulfield DF. A Chemical Kinetics Approach to The Duration-of-Load Problem in Wood. Wood and Fiber Science 1985;17:504–21.